

**KERNFORSCHUNGSZENTRUM  
KARLSRUHE**

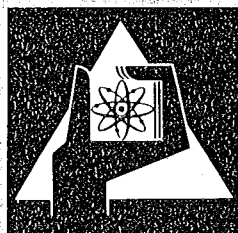
November 1974

KFK 2077

Institut für Angewandte Systemtechnik und Reaktorphysik  
Projekt Schneller Brüter

**Control Rod Worth and Power Distribution Measurements  
in the SNR Mock up SNEAK Assembly 9A**

M. Pinter, R. Böhme, G. Durance, P. Fehsenfeld,  
H. Giese, S. Pilate, U. Wehmann



**GESELLSCHAFT  
FÜR  
KERNFORSCHUNG M.B.H.**

**KARLSRUHE**

Als Manuskript vervielfältigt

Für diesen Bericht behalten wir uns alle Rechte vor

GESELLSCHAFT FÜR KERNFORSCHUNG M. B. H.  
KARLSRUHE

KERNFORSCHUNGSZENTRUM KARLSRUHE

1974

KFK 2077

Institut für Angewandte Systemtechnik und Reaktorphysik  
Projekt Schneller Brüter

Control rod worth and power distribution measurements  
in the SNR mock up SNEAK assembly 9A

M. Pinter, R. Böhme, G. Durance<sup>1)</sup>, P. Fehsenfeld,  
H. Giese, S. Pilate<sup>2)</sup>, U. Wehmann<sup>3)</sup>

- 1) Delegate from AAEC, Sydney, Australia
- 2) Belgonucleaire, Brussels
- 3) Interatom, Bensberg

Gesellschaft für Kernforschung mbH., Karlsruhe



Control rod worth and power distribution measurements in  
the SNR mock up SNEAK-Assembly 9A

Abstract

The series of assemblies which were built for investigations with regard to the SNR was continued with the Assembly SNEAK-9A. This assembly was a mock up of the SNR with two core zones in the radial direction. The fuel material was enriched uranium. The main objectives were control rod worths and power distribution measurements. Most of the calculations were performed with the group diffusion method using 4 energy groups. The most important result is a general underestimate of the control rod worths. The power distribution shows in general an overestimate in the upper, and an underestimate in the lower core half. This effect may also be related to the underestimate of the control rod worths.

18.10.1974

Messung der Kontrollstabwerte und der Leistungsverteilung  
in der SNR-Nachbildung SNEAK-9A

Zusammenfassung

Die Reihe der Anordnungen, die im Zusammenhang mit Untersuchungen für den SNR aufgebaut wurden, wurde mit dem SNR-mock-up SNEAK-9A fortgesetzt. Das Core bestand aus zwei verschieden angereicherten radialen Zonen mit Uran als Brennstoff. Hauptziel der Untersuchungen war die Bestimmung des Reaktivitätswertes von simulierten Kontrollstäben mit Hilfe von unterkritischen Messungen, sowie die Messung von dreidimensionalen Leistungsverteilungen bei verschiedenen Stellungen der Kontrollstäbe. Zur Nachrechnung der Experimente wurde größtenteils die Gruppendiffusionsmethode mit 4 Energiegruppen verwendet. Das wichtigste Ergebnis ist eine generelle Unterschätzung der Kontrollstabwerte. Die Leistungsverteilung zeigt im allgemeinen eine Überschätzung in der oberen und eine Unterschätzung in der unteren Corehälfte. Dieser Effekt ist wahrscheinlich ebenfalls auf die Unterschätzung der Kontrollstabwerte zurückzuführen.

## Table of Contents

	Page
1. Introduction	1
2. Description of the assembly	3
3. Measurement of control rod worths	8
3.1 Summary of the experiments performed	8
3.2 The subcritical source multiplication measurements	9
3.3 The subcritical source jerk measurements	11
3.4 The quasicritical measurements	16
4. Calculation of control rod worths	20
4.1 Methods of calculation	20
4.1.1 Use of the KASY synthesis method	20
4.1.2 Values used for $\beta_{\text{eff}}$	22
4.2 Direct results of calculations (subcritical cases)	23
4.2.1 Presentation; effect of few group condensation	23
4.2.2 Comparison KFKINR - MOXTOT	26
4.3 Comments on the C/E ratios (subcritical cases)	27
4.3.1 Main results of SNEAK-9A	27
4.3.2 Note on transport results	30
4.4 Evaluation of the quasicritical measurements	31
4.4.1 Characteristic curves of control rods	31
4.4.2 Simulation of dummy assemblies for the SNR	33

	Page
5. Measurement of fission rate maps (power mapping)	37
5.1 General marks	37
5.2 Fission chamber measurements	37
5.3 Activation measurements	39
5.4 Comparison of the techniques	41
6. Calculation of the fission rate maps	43
6.1 Description of the calculations	43
6.1.1 Basic methods used	43
6.1.2 Normalization of fission rates	45
6.2 Basic results of the evaluation	47
6.2.1 $k_{eff}$ values	47
6.2.2 Power mapping evaluation for the first core (40/40)	48
6.2.3 Power mapping evaluation for the two other cores (28/50, 58/20)	53
6.3 Check of methods	57
6.3.1 Effect of mesh spacing, of blanket trial functions and of condensation	57
6.3.2 Notes on cross-section set influence and transport results	61
References	62
Appendix A	65
Figures	68



## 1. Introduction

The critical assembly SNEAK-9A was built with the main purpose to study the effectiveness of the control system of the planned prototype SNR-300 and to improve the prediction of the power distribution for various control rod insertion patterns. In previous SNEAK assemblies /9/,/16/ similar experiments have been performed. However, only a limited number of control rods was studied at each time. In the present work an effort was made to approach as closely as possible the geometry of the SNR, including a simulation of all the control rods. Also the compositions of the two core zones were approximated as well as possible. However, because of the insufficient plutonium supply at SNEAK, only enriched uranium was used as fuel. The axial blanket had a composition similar to a breeder blanket, in the radial blanket depleted uranium blocks were used.

The reference design of the SNR-300 /17/ which was to be simulated in SNEAK has a core height of 95 cm, a core radius of 77.4 cm and contains two concentric enrichment zones of respective enrichments 19 and 26% (fissile Pu/U+Pu). The axial and radial blankets contain mainly depleted uranium oxide, sodium, and structural steel; they are 40 cm thick axially and 20 cm thick radially. (Table 2.1 gives the atomic densities of the different zones, Fig. 1 shows a horizontal section through the reactor.)

The control rod system consists of 9 compensating rods and 3 safety rods positioned approximately along two rings as shown in Fig. 1. Both types of rods are loaded with enriched  $B_4C$ . While the safety rods are always withdrawn during normal operation the compensating rods are about half inserted at the beginning of a burnup cycle and are gradually withdrawn as burnup proceeds. The combined reactivity of the three inner compensating rods is about equal to that

of the six outer ones. All nine compensating rods represent a total reactivity of about 7.5%. The safety rods provide further 3.6%.

Since the inception of SNEAK-9A the design for the SNR has undergone some changes. The core radius is now planned to be increased to 89.5 cm, the surplus reactivity being compensated at the beginning of life by using diluent rods in some of the fuel element positions. Such a configuration permits a considerably higher burnup.

Although this redesign was not taken into account by the SNEAK-9A lay-out, the features of the assembly are still close enough even to the present design of the SNR to give useful results.

The evaluation of the experiments made in SNEAK-9A is performed using the standard calculation methods employed for the SNR designs: KFKINR cross-section set /7/, and diffusion theory in 3 dimensions (XYZ) with the help of the synthesis approach /2/, /3/. Complementary calculations are also made using former cross-section sets and using transport theory.

For the SNR designers the direct goals of SNEAK-9A are therefore to provide correction factors, based on the calculation-to-experiment ratios found in SNEAK, for the following SNR core characteristics:

- $k_{eff}$  of cores containing control rods inserted according to different policies, representative of the SNR-300 at beginning and at end of life (this topic is more specially treated in the companion report KFK-2028 /1/);
- reactivity worths of the different groups of control rods;

- parameters of the power distribution in the core for various rod insertion patterns.

The results of these experiments will aid in determining for the SNR-300 the fuel enrichments in both core zones and the  $^{10}\text{B}$  content of the absorber rods, and in planning the insertion policy during burnup.

The work presented here with full details was already shortly described in /6/.

## 2. Description of the assembly

Both assemblies, SNEAK-9A-1 and 9A-2 contained two cylindrical core regions with a height of 90.0 cm, a radial blanket about 30 cm thick, and an upper and lower axial blanket 40.8 cm thick.

In designing the unit cells for SNEAK-9A an effort was made to approach the compositions and spectra in the respective zones of the SNR as well as possible<sup>+)</sup> . However, the cell also had to be kept reasonably simple in order to allow a meaningful interpre-

---

<sup>+)</sup>  Special attention was payed to the  $^{10}\text{B}$ -worth.

tation, in particular of the reaction rate measurements. As a fuel, 20.04% enriched uranium was used in the inner zone and 35.28% enriched uranium in the outer zone.

In the axial blanket a breeder composition was approximated. Because of the lack of  $UO_2$  platelets this had to be done using two different unit cells. Over a thickness of about 20 cm immediately adjacent to the core a composition containing mainly  $UO_2$  and Na was used (inner axial blanket). For the remaining part of the blanket a cell containing natural uranium,  $Al_2O_3$ , Al, and stainless steel was used (outer axial blanket). The radial blanket consisted of depleted uranium with a content of 0.41%  $^{235}U$ .

In Table 2.1 the atomic compositions used for the calculations are summarized. More details, especially the unit cells and the structure of the core elements are given in /1/.

The main characteristic of these assemblies is that they contain simulated SNR control rods. There were twelve SNR control rod positions, which were divided into 3 groups:

- RT1 consisting of three control rods positioned in the inner core zone at about one third of the core radius.
- RT2 consisting of six control rods positioned in the outer core zone but directly adjacent to the inner core zone.
- A secondary shut-down system, consisting of three rods, positioned in the inner core zone between RT1 and RT2.

Table 2.1 Atomic compositions ( $10^{22}$  atoms/cm<sup>3</sup>)

Part A: SNR-300 preliminary design data

Mixture Isotope	Inner core zone	Outer core zone	Breeder blanket	Control rod	
				absorber part	follower part
<sup>10</sup> B	--	--	--	0.8639	--
<sup>11</sup> B	--	--	--	1.0558	--
C	0.0077	0.0077	0.0077	0.4799	--
Cr + Mn	0.3057	0.3057	0.3063	0.5953	0.2409
Fe	1.0404	1.0404	1.0422	1.9196	0.7766
Ni	0.2644	0.2644	0.2649	0.4833	0.1955
O	1.1573	1.1618	1.2880	--	--
Na	1.0829	1.0829	1.0486	0.9452	1.9272
<sup>235</sup> U	0.0011	0.0010	0.0016	--	--
<sup>238</sup> U	0.4541	0.3983	0.6522	--	--
<sup>239</sup> Pu	0.0992	0.1428	--	--	--
<sup>240</sup> Pu	0.0291	0.0419	--	--	--
<sup>241</sup> Pu	0.0033	0.0048	--	--	--
<sup>242</sup> Pu	0.0007	0.0010	--	--	--

Table 2.1 Atomic compositions ( $10^{22}$  atoms/cm<sup>3</sup>)

Part B: Used in the SNEAK-9A calculations

Mixture Isotope	Core inner zone R1		Core outer zone R2		B <sub>4</sub> C absorber rod	Na follower rod	Radial blanket	Axial blanket	
	pure cell	homogenized for k <sub>eff</sub> calculation	pure cell	homogenized for k <sub>eff</sub> calculation				inner	outer
Al	--	0.06257	--	0.02681	2.1170	--	0.4019	0.2615	1.4263
<sup>10</sup> B	--	--	--	--	0.4091	--	--	--	--
<sup>11</sup> B	--	--	--	--	1.6787	--	--	--	--
C	1.0495	1.0456	1.4590	1.4592	0.5233	0.003721	0.000299	0.004530	0.002044
Cr + Mn	0.2666	0.2691	0.2527	0.2532	0.1196	0.3171	0.02637	0.2685	0.2190
Fe	0.9072	0.9151	0.8569	0.8581	0.3984	1.0769	0.08714	0.9074	0.7255
H	0.002599	0.002606	0.001189	0.001186	--	--	--	0.000615	--
K	0.000273	0.000275	0.000125	0.000125	--	--	--	--	--
Mg	--	0.000641	--	0.000275	--	--	0.002924	0.002886	0.009645
Mo	0.001514	0.001420	0.001706	0.001658	0.000997	0.002415	0.000220	0.001956	0.000997
Na	1.2729	1.2353	1.1385	1.1143	--	1.6671	--	0.6653	--
Nb	0.000854	0.000804	0.000854	0.000830	0.000854	0.000854	0.000188	0.000874	0.000854
Ni	0.1485	0.1485	0.1477	0.1473	0.05724	0.1854	0.05383	0.1439	0.1152
O	1.0026	1.0087	0.4587	0.4581	--	0.000031	--	1.3979	1.1597
Si	0.01144	0.01197	0.01159	0.01177	0.00863	0.01621	0.001895	0.01445	0.01496
Ti	--	0.000228	--	0.000110	--	--	0.000046	--	0.001818
<sup>235</sup> U	0.14892	0.14763	0.23979	0.23972	--	--	0.016245	0.004992	0.005828
<sup>238</sup> U	0.59392	0.58879	0.43933	0.43922	--	--	3.9940	0.68833	0.80313

Each simulated control rod consisted of four SNEAK elements. To be able to adapt its reactivity worth as accurately as possible to a given value, the SNEAK elements were filled in the absorber part with a pattern of four by four rodlets part of which were  $B_4C$  filled aluminium tubes, the rest consisting of solid aluminium. Each of them had a diameter of 12 mm.

To reduce the free space between these tubes and rodlets smaller aluminium rodlets with a diameter of 5 mm were used. The final version used in SNEAK-9A-1 and SNEAK-9A-2 consisted of 12  $B_4C$  tubes (diameter 12 mm), 4 aluminium rodlets (diameter 12 mm), and 9 aluminium rodlets (diameter 5 mm) per SNEAK element. A cross section is shown in Fig. 2.

In the follower part of the control rods normal SNEAK sodium platelets were used.

In the assembly SNEAK-9A-1 all twelve control rods were simulated in the withdrawn condition. That means, there was follower material in the core region and the lower axial blanket, and absorber material in the region of the upper axial blanket. Thus the assembly corresponded to the end of life configuration of the SNR.

SNEAK-9A-2 was a mock up of a possible begin of life configuration of the SNR-300. In the reference core all nine compensating rods were simulated 40 cm inserted, i.e. the boundary between absorber and follower part of the control rods was 40 cm below the upper core blanket boundary. The shut-down rods were still simulated withdrawn. The loss of reactivity by inserting the nine rods was compensated by additional core elements.

In addition to this reference core with insertion depths of 40/40 cm of the two control rod systems RT1 and RT2 respectively, four modifications of SNEAK-9A-2 have been built. All these cores had the same radii but only changed insertion depths of the control rods: 58/20, 28/50, 0/63, and 68/0 cm.

The horizontal cross-sections of the critical assemblies SNEAK-9A-1 and 9A-2 are shown in Fig. 3.

### 3. Measurement of control rod worths

#### 3.1 Summary of the experiments performed

Control rod worth experiments were performed in both assemblies SNEAK-9A-1 and SNEAK-9A-2.

In SNEAK-9A-1 the characteristic of the inner control rod bank RT1, and two states with all nine control rods inserted to the same level, were measured by means of the subcritical source multiplication method.

In SNEAK-9A-2 three types of experiments were performed:

- Measurement of the characteristic of the control rod banks RT1 and RT2 separately and both together respec-



tively, starting from the critical reference position RT1/RT2 equal 40/40 cm inserted to the full insertion depth of about 90 cm.

These measurements were performed by means of the subcritical source multiplication method, and the subcritical source jerk technique.

- Measurement of the characteristic near the critical insertion depth of one single control rod of both RT1 and RT2 control rod bank, and of two symmetrical RT2 rods. These measurements were performed for different critical core configurations, i.e. RT1/RT2 equal 40/40, 0/63, and 68/0 cm respectively. The quasicritical method was used in this case.
  
- Measurement of the radial dependence of the reactivity worth of one rod filled with sodium or boron carbide respectively, simulating a SNR diluent subassembly. Again the quasicritical method was used.

### 3.2 The subcritical source multiplication measurements

The source multiplication method is, from the experimental point of view, the simplest technique to determine the reactivity state of a subcritical core configuration, if it is possible to calibrate the method at one subcritical state with a known reactivity. It

is only necessary to have a fixed neutron source and a neutron detector anywhere in the reactor, and to record the counting rate for each subcritical state to be measured.

However, the very simple evaluation based on the point reactor model is no longer valid, if there appear significant variations in the profiles of the real and the adjoint fluxes as a consequence of the reactivity change for instance by inserting a control rod. As it is shown in Appendix A, a calculated correction factor must be applied to the measured result.

In the special case of SNEAK-9A, a  $^{252}\text{Cf}$ -source was placed in the core center, and the neutron flux was recorded by two ionization chambers and two  $^3\text{He}$ -counters positioned far away from the core center at the outer blanket boundary (see Fig. 9). The calibration of the method was performed by inserting a calibrated SNEAK shim rod. Two different reactivity states were used, i.e. 19.8  $\rho$  and 62.5  $\rho$ . The agreement of the calibration factors was better than 2% for each detector.

The agreement of the results obtained by the four detectors was in many cases better than 1% and for all cases better than 3%. These deviations are systematical ones and probably caused by a slightly different influence of the control rod movement on to the flux changes at the four detector positions.

The correction factor, which was to be applied to each measured result, was calculated by the following way. Two dimensional inhomogeneous diffusion runs with the DIXY code in (R-Z)-geometry were made first. In this way it was possible to calculate the change of the effective source strength and of the detector efficiency (see Appendix A) as function of the insertion depth of

the control rod banks. Then a cylinderization correction was determined by comparing two dimensional DIXY calculations in (X-Y)-geometry with one dimensional calculations in cylinder geometry using the same axial buckling. For all calculations the KFKINR cross-section set was used with a 4 energy group scheme. The final results of these calculations for the measurements in SNEAK-9A-2 are given in Table 3.1. The correction factors needed to improve the measurements resulted by interpolation of the calculated values  $F_{XY}$  (last column in Table 3.1).

Qualitatively one can see from Table 3.1, that the insertion of the RT1 bank decreases the source strength, while the insertion of the RT2 bank mainly diminishes the detector efficiency.

In Table 3.2 the results of the measurements with and without calculated corrections are given for the experiments in SNEAK-9A-1 and SNEAK-9A-2. The errors also given in Table 3.2 consist of two parts: 3% are coming from the calibration of the method and more over it was assumed that the correction factor may have an error of 20%.

### 3.3 The subcritical source jerk measurements

With the source jerk technique the subcriticality of a system is derived from the time dependent neutron flux signal of a neutron detector, caused by a change of the source strength of a neutron source in the subcritical system.

Table 3.1      Calculated correction factors for the source multiplication measurement in SNEAK-9A-2

Control rod insertion depth (cm) RT1/RT2/A	Effective source strength $S_{eff}^{+)}$		Detector efficiency $W^{+)}$		Total correction factor $W \cdot S_{eff}^{+)}$	
	DIXY (R-Z)	DIXY (R-Z) + cyl.corr.	DIXY (R-Z)	DIXY (R-Z) + cyl.corr.	$F_{RZ}$	$F_{XY}$
40/40/0	1.000	1.000	1.000	1.000	1.000	1.000
48.6/40/0	0.964	0.967	0.999	0.997	0.963	0.964
70/40/0	0.909	0.914	0.998	0.993	0.907	0.908
90/40/0	0.900	0.906	0.999	0.992	0.899	0.899
40/48.6/0	1.008	1.003	0.980	0.985	0.987	0.988
40/61.5/0	1.019	1.010	0.952	0.963	0.971	0.973
40/74/0	1.028	1.018	0.937	0.949	0.963	0.966
40/90/0	1.032	1.021	0.932	0.945	0.961	0.965
48.6/48.6/0	0.971	0.969	0.978	0.982	0.950	0.952
61.5/61.5/0	0.943	0.940	0.950	0.960	0.896	0.902
74/74/0	0.935	0.931	0.935	0.946	0.874	0.881
90/90/0	0.933	0.929	0.931	0.943	0.869	0.876
90/90/90	0.890	0.881	0.908	0.951	0.808	0.838
40/40/90	0.948	0.946	0.978	0.995	0.927	0.941
0/61.5/90	1.034	1.026	0.929	0.964	0.960	0.989
70/0/90	0.846	0.855	1.021	1.023	0.863	0.875

+ ) Relative to the reference configuration 40/40/0.

Table 3.2

Experimental results of the control rod worth measurement in SNEAK-9A-1 and SNEAK-9A-2 performed with the source multiplication method

SNEAK-9A-1				SNEAK-9A-2			
Control rod insertion depth (cm) RT1/RT2/A	$\rho_{\text{meas.}}$ (%)	Corr. factor F	$\rho_{\text{corr.}}$ (%)	Control rod insertion depth (cm) RT1/RT2/A	$\rho_{\text{meas.}}$ (%)	Corr. factor F	$\rho_{\text{corr.}}$ (%)
15/0/0	0.51	0.995	0.51±0.02	45/40/0	0.42	0.976	0.41±0.02
30/0/0	1.52	0.976	1.48±0.05	50/40/0	0.86	0.957	0.82±0.03
40/0/0	2.41	0.949	2.29±0.09	60/40/0	1.74	0.924	1.61±0.07
45/0/0	2.94	0.934	2.75±0.12	70/40/0	2.53	0.907	2.29±0.11
50/0/0	3.46	0.917	3.17±0.15	80/40/0	3.06	0.901	2.76±0.14
60/0/0	4.53	0.891	4.04±0.21	90/40/0 <sup>+) )</sup>	3.36	0.900	3.02±0.15
75/0/0	5.73	0.876	5.02±0.27	40/45/0	0.46	0.992	0.46±0.02
90/0/0 <sup>+) )</sup>	6.25	0.871	5.44±0.29	40/50/0	0.93	0.986	0.92±0.03
40/40/0	4.62	0.926	4.28±0.19	40/60/0	1.87	0.975	1.82±0.06
45/45/0	5.61	0.903	5.07±0.25	40/70/0	2.65	0.968	2.57±0.09
SNEAK-9A-2				40/80/0	3.24	0.966	3.13±0.11
				40/90/0 <sup>+) )</sup>	3.54	0.965	3.42±0.13
SNEAK-9A-2				45/45/0	0.89	0.972	0.87±0.03
				50/50/0	1.83	0.946	1.73±0.07
40/40/90 <sup>+) )</sup>	4.54	0.941	4.27±0.18	60/60/0	3.77	0.908	3.42±0.16
0/63/90 <sup>+) )</sup>	4.62	0.989	4.57±0.15	70/70/0	5.47	0.886	4.85±0.26
68/0/90 <sup>+) )</sup>	4.60	0.877	4.03±0.22	80/80/0	6.71	0.878	5.89±0.32
90/90/90 <sup>+) )</sup>	12.80	0.838	10.73±0.67	90/90/0 <sup>+) )</sup>	7.31	0.876	6.40±0.35

<sup>+) )</sup> The nominal insertion depth of 90 cm means, that the control rod with an absorber height of 88.6 cm is positioned symmetrically to the core midplane.

Two different experimental techniques were used. In the first technique a Cf source with a strength of  $4 \times 10^7$  n/sec was placed in the pile oscillator close to the core center position which allowed to move the source in or out of the reactor in about 1 second.

In the second technique a pulsed neutron generator was used. A duoplasmatron ion source producing deuterium ions was placed outside the reactor and a drift tube with a tritium target at its end extended to the core center. 14 MeV neutrons were produced at the target by the  ${}^3\text{T}(d,n){}^4\text{He}$  reaction. In its normal operation the source was pulsed with a frequency of 500/sec and a yield of up to  $5 \times 10^5$  neutrons/pulse. For evaluation purposes this was considered as a continuous source. The source strength was then about  $2 \times 10^8$  n/sec. The "source jerk" was achieved by simply switching off the generator.

Comparing the two techniques it showed that the operation of the neutron generator was much more difficult than the operation with the pile oscillator, and only a part of the subcritical core configurations could therefore be measured with the pulse generator. On the other hand, using the pile oscillator, it showed that a correction to the measured detector signals had to be applied due to the fact that neutrons reached the detectors on a way outside the core, when the neutron source is in the out of core position.

All source jerk measurements were evaluated using the inverse kinetics equations. As one can see from Table 3.3 the results of both techniques are very consistent after correcting the pile oscillator results. However there remained big discrepancies between the source jerk and the source multiplication results especially for large subcritical states.

Table 3.3 Detailed results of the source jerk measurements

Control rod insertion depth (cm) RT1/RT2/A	Oscillated <sup>252</sup> Cf-source measured ( § )	with back- ground corr. ( § )	Neutron generator measured ( § )	Mean value ( § )	Mean value corrected due to higher modes ( § )
45/40/0	0.409	0.412	0.405	0.409	0.41 ± 0.01
50/40/0	0.819	0.826	0.826	0.826	0.83 ± 0.02
60/40/0	1.57	1.60	1.60	1.60	1.63 ± 0.05
70/40/0	2.16	2.21	2.24	2.23	2.30 ± 0.09
80/40/0	2.61	2.70	--	2.70	2.81 ± 0.12
90/40/0	2.75	2.84	2.88	2.86	2.98 ± 0.14
40/45/0	0.439	0.442	--	0.442	0.44 ± 0.01
40/50/0	0.898	0.906	--	0.906	0.92 ± 0.02
40/60/0	1.73	1.77	--	1.77	1.80 ± 0.05
40/70/0	2.41	2.47	--	2.47	2.55 ± 0.09
40/80/0	2.81	2.91	--	2.91	3.04 ± 0.14
40/90/0	3.07	3.21	3.21	3.21	3.37 ± 0.16
45/45/0	0.853	0.860	--	0.861	0.87 ± 0.02
50/50/0	1.68	1.71	--	1.71	1.74 ± 0.05
60/60/0	3.18	3.30	--	3.30	3.45 ± 0.17
70/70/0	4.31	4.54	4.56	4.55	5.0 ± 0.3
80/80/0	5.06	5.40	--	5.40	5.9 ± 0.4
90/90/0	5.42	5.84	5.86	5.85	6.5 ± 0.5
40/40/90	3.74	3.90	3.93	3.92	4.15 ± 0.22
0/63/90	3.83	4.14	4.10	4.12	4.35 ± 0.24
68/0/90	3.51	3.68	3.74	3.71	3.90 ± 0.21
90/90/90	7.69	8.67	8.82	8.74	10.5 ± 1.1

Further investigations showed that also for the detectors far away from the core the contributions of the higher spatial modes could not be neglected. But fortunately the higher modes die out according to the prompt neutron lifetime. As a consequence the time dependent neutron flux after the prompt jump is not influenced. Therefore it is sufficient to apply a correction to the stable signal of the flux detectors before the ejection of the neutron source. However it showed that it was not possible to calculate accurately the contribution of the higher modes with a justifiable expense on computer time. Therefore the correction factor was derived from analytical calculations of a bare cylinder reactor. The results obtained by this procedure and given in the last column of Table 3.3 may be rather inaccurate, but as some one- and two-dimensional calculations approximating the real core geometry yielded correction factors of the same magnitude, this procedure seemed to be reasonable.

Moreover the accuracy of the correction factors is assumed to be about 30%, and for comparisons with the calculated results the more accurate source multiplication results have been used.

#### 3.4 The quasicritical measurements

The quasicritical method is the most proper method for measuring small reactivity changes. SNEAK shim rods were calibrated with the inverse kinetics procedure and then used to compensate the reactivity change which should be measured.

The limits of this method are twofold:



Because of safety injunctions the excess reactivity in the core must not exceed 1%  $\Delta k$ . Nevertheless it is often possible to measure a larger reactivity change stepwise by loading or unloading edge elements. But this procedure may influence the reactivity worth to be measured, if the core size changes too much.

The accuracy attainable with the quasicritical method is in general about 3 to 5% but may be better than 2% in special cases (compared with stable period measurements for small reactivities).

Two kinds of experiments have been performed with this method.

First, in the three core configurations of SNEAK-9A-2 (40/40, 28/50, and 58/20) the reactivity characteristic near the critical insertion depth of one RT1-, one RT2-, and two symmetrical RT2-control rods was measured. As the measured reactivity changes were less than  $\pm 30 \text{ } \mu$ , all measurements could be performed in a core with 538 core elements.

The results of these measurements are given in Table 3.4. First of all the comparison of these data to calculated ones is interesting (see section 4.4.1), but comparing the RT2-results for one and two control rods, also a self-shielding effect of about 4% can be deduced.

Another experiment was also performed with the quasicritical technique.

The initial core (Mark Ia) of the SNR-300 will be overenriched for different reasons. As this overreactivity is too large to be compensated by the normal control rod system, some normal fuel elements will be replaced by special dummy elements also called "diluent".

Table 3.4 Measurement of the reactivity characteristic of single control rods near the critical insertion depth

RT1-control rod		RT2-control rods		
insertion depth (cm)	$\rho$ ( $\epsilon$ )	insertion depth (cm)	$\rho$ ( $\epsilon$ )	
	one rod		one rod	two symm. rods
31	+ 22.7	31	+ 12.7	+ 24.2
34	+ 15.7	34	+ 8.7	+ 16.5
37	+ 8.3	37	+ 4.6	+ 8.4
<b>40</b>	reference	<b>40</b>	reference	reference
43	- 8.6	43	- 4.3	- 8.9
46	- 17.1	46	- 9.0	- 17.6
49	- 25.9	49	- 13.4	- 26.8
19	+ 17.5	41	+ 14.3	+ 27.2
22	+ 12.3	44	+ 9.6	+ 18.4
25	+ 6.5	47	+ 4.7	+ 9.2
<b>28</b>	reference	<b>50</b>	reference	reference
31	- 7.4	53	- 4.9	- 9.0
34	- 15.1	56	- 9.3	- 17.9
37	- 23.2	59	- 13.6	- 26.3
49	+ 24.7	11	+ 7.3	not measured
52	+ 16.3	14	+ 5.1	
55	+ 8.1	17	+ 2.8	
<b>58</b>	reference	<b>20</b>	reference	
61	- 8.1	23	- 3.1	
64	- 15.4	26	- 6.7	
67	- 22.1	29	- 10.4	

Table 3.5 Radial dependence of the reactivity worth of Na- and B<sub>4</sub>C-dummy elements

Nr.	Position core plane X / Y	$\rho$ ( $\phi$ )	
		sodium <sup>1)</sup>	B <sub>4</sub> C <sup>2)</sup>
1	17,18 / 20,21	57.2	<u>244.0</u>
2	" / 18,19	56.4	235.9
3	" / 24,25	52.0	217.1
4	" / 28,29	40.9	153.7
5	" / 10,11	53.8	128.6
6	" / 9,10	47.8	103.0
7	" / 8,9	40.5	75.6
8	" / 12,13	42.0	154.8
9	" / 13,14	45.0	173.4

- 1) Core size: 538 core elements  
control rod insertion depth RT1/RT2: 37/37 cm
- 2) Core size: 538 core elements  
control rod insertion depth RT1/RT2: 26/26 cm

In SNEAK-9A-2 therefore the radial dependence of the reactivity worth of two kinds of such dummy elements (one containing sodium, the other absorber material like the compensating rods) was measured. The measuring positions are shown in Fig. 4 together with the core layout of the SNR-300. The results of the experiments are given in Table 3.5.

#### 4. Calculation of control rod worths

##### 4.1 Methods of calculation

##### 4.1.1 Use of the KASY synthesis method

The method used was basically the same as used in all SNEAK control rod evaluations: diffusion theory, few group cross-sections, 3D (XYZ) geometry using the flux synthesis program KASY /2/,/3/.

The following minor points are to be mentioned:

- the atom densities used correspond to  $k_{\text{eff}}$  calculations, i.e. the SNEAK shim and safety rods are mixed with the pure fuel zones (see Table 2.1);
- the cross-sections are calculated for the homogeneous media;
- the core size corresponds to 540 core elements as in the actual core; the influence of the measuring channel was neglected.

Two series of calculations were performed independently, with two different cross-section sets:

KFKINR cross-sections condensed in a four groups scheme: (4,6,10,26 according to the standard Russian structure);

MOXTOT cross-sections condensed in six groups: (4,6,8,10,12,26).

In addition, a few calculations were also repeated with MOXTOT (four and twelve groups) and KFKINR (six groups).

Let be:

$k_1$  the  $k_{\text{eff}}$  value calculated for the reference core (critical);

$k_2$  the  $k_{\text{eff}}$  value calculated for the subcritical one.

The reactivity  $\rho$  is given by:

$$\rho = \frac{k_1 - k_2}{k_2}$$

Due to inaccuracies in the cross-section sets and calculation methods,  $k_1$  is not calculated exactly equal to unity; the error is supposed to affect both  $k_{\text{eff}}$  values  $k_1$  and  $k_2$  by the same factor.

In the results here presented, the error in  $k_1$  is always smaller than 1%.

The KASY synthesis calculations used basically trial functions representative of the different 2D (XY) slices delimited in the core by the insertion of the control rods, e.g. 2 functions for the characteristic (RT1 + RT2), or 3 functions for the characteristic of the safety rods A.

It was observed that adding a blanket trial function when calculating the start and end  $k_{\text{eff}}$  values had practically no effect: the modification in the method affects equally both values. This confirms the results of the detailed investigation on the influence of blanket trial functions made by C. Hoenraet and S. Pilate.

The following problem associated with the choice of trial functions was also examined. In general, exactly the same set of trial functions was used for calculating the different points of a characteristic curve, in particular also for the start point. Since the synthesis gives an approximate solution, the start-up  $k_{\text{eff}}$  value for 40/40 is not exactly constant, when calculated with different sets of core trial functions. But this effect was found to be negligible, except for the characteristic of the safety rods for which it reached 1% relative.

#### 4.1.2 Values used for $\beta_{\text{eff}}$

For the sake of comparing experimental (in  $\rho$ ) and calculated (in  $\Delta k/k$ ) reactivities, the following  $\beta_{\text{eff}}$  values are assumed:

0.715% for SNEAK-9A-1;

0.710% for SNEAK-9A-2

(except 0.703% for the case 90/90/90).

The  $\beta_{\text{eff}}$  values used were calculated by perturbation in 2D (RZ) geometry on the basis of the yields of delayed neutron per fission due to Keepin /4/ and of the  $\bar{\nu}$  values calculated for SNEAK-9A (see also section 4 of Ref. /1/).

There exists a variation of  $\beta_{\text{eff}}$  throughout the experiments, due to flux and importance shifts caused by the insertion of the control rods. From (RZ) calculations, the maximum amplitude of this

variation, from the case 40/40/0 to the case 90/90/90, is only -1% relative. Its effect was therefore neglected.

It is to be noticed that the choice of the basic  $\beta_{eff}$  data has a direct influence on the whole evaluation. As an example, an increase of  $(\nu\beta)$  for  $^{238}\text{U}$  by 10% relative as suggested by Tomlinson /5/ should result for SNEAK-9A in a  $\beta_{eff}$  2% higher and therefore in C/E ratios for control rod worths 2% lower.

#### 4.2 Direct results of calculations (subcritical cases)

##### 4.2.1 Presentation; effect of few group condensation

The results of calculations are presented in Table 4.1 (SNEAK-9A-1) and Table 4.2 (SNEAK-9A-2); these tables are similar to tables IV and V of /6/, but some figures have been slightly revised after checks. The measured results quoted are relative to the source multiplication method only, as mentioned in section 3.3.

Due to the presence of bottom and top plugs, the active length of the absorber rod is not 90 cm but 88.6 cm. The calculation results were accordingly corrected for the case of full insertion; for the RT rods, this correction amounts to -1% relative.

With respect to 26 group results,  $k_{eff}$  is modified due to condensation by less than  $10^{-3}$  with 6 groups and  $2 \times 10^{-3}$  with 4 groups. This modification is positive (increase) for cases of large absorber insertion and negative (decrease) for cases of large rod withdrawal.

Table 4.1 Comparison between measured and calculated reactivity worths for various control rod configurations in SNEAK-9A-1

Insertion depth of RT1/RT2 (cm)	Measured (source multiplication) ( $\Delta k/k$ )	Calculated KASY (XYZ) ( $\Delta k/k$ )		C/E ratios	
		KFKINR four groups	MOXTOT six groups	KFKINR four groups	MOXTOT six groups
15/0	0.00364	0.00309	0.0033	0.85	0.91
30/0	0.0106	0.00952	0.0104	0.90	0.98
40/0	0.0164	0.0153	0.0164	0.93	1.00
45/0	0.0197	0.0184	0.0194	0.93	0.98
50/0	0.0227	0.0215	--	0.95	--
60/0	0.0288	0.0274	0.0286	0.95	0.99
75/0	0.0359	0.0341	0.0356	0.95	0.99
90/0	0.0389	0.0367	0.0385	0.94	0.99
40/40	0.0305	0.0288	--	0.94	--
45/45	0.0363	0.0350	0.0372	0.97	1.02



Table 4.2

Comparison between measured and calculated reactivity worths  
for various control rod configurations in SNEAK-9A-2

Rod configuration RT1/RT2/A (cm)	Measured (source multiplication) ( $\Delta k/k$ )	Calculated KASY (XYZ) ( $\Delta k/k$ )		C/E ratios	
		KFKINR four groups	MOXTOT six groups	KFKINR four groups	MOXTOT six groups
45/40/0	0.00290	0.00264	--	0.91	--
50/40/0	0.00582	0.00542	--	0.93	--
60/40/0	0.0114	0.0106	0.0112	0.93	0.98
70/40/0	0.0163	0.0150	--	0.92	--
80/40/0	0.0196	0.0179	0.0190	0.91	0.97
90/40/0	0.0214	0.0193	0.0210	0.90	0.98
40/45/0	0.00327	0.00301	--	0.92	--
40/50/0	0.00653	0.00598	--	0.92	--
40/60/0	0.0129	0.0119	0.0123	0.92	0.95
40/70/0	0.0182	0.0168	--	0.92	--
40/80/0	0.0222	0.0203	0.0210	0.91	0.95
40/90/0	0.0243	0.0217	0.0229	0.89	0.94
45/45/0	0.00618	0.00570	--	0.92	--
50/50/0	0.0123	0.0114	--	0.93	--
60/60/0	0.0243	0.0227	0.0240	0.93	0.99
70/70/0	0.0344	0.0322	--	0.94	--
80/80/0	0.0418	0.0385	0.0408	0.92	0.98
90/90/0	0.0454	0.0413	0.0439	0.91	0.97
40/40/90	0.0302	0.0272	0.0289	0.90	0.96
0/63/90	0.0325	0.0284	0.0304	0.87	0.94
68/0/90	0.0286	0.0256	0.0273	0.90	0.95
90/90/90	0.0755	0.0677	0.0721	0.90	0.96

The values of control rod reactivity worths calculated with few group cross-sections are therefore reduced with respect to 26 group results.

For the cases considered here, the use of 4 groups instead of 6 changes the reactivity worths by:

$$- 2 \pm 1\% \quad (\text{depending on the case}),$$

and the use of 6 groups instead of 12 by less than -1%.

#### 4.2.2 Comparison KFKINR - MOXTOT

One observes from Table 4.1 and Table 4.2 that the KFKINR (4 groups) results are 5 to 6% lower than the MOXTOT (6 groups) results.

The relative deviations are indeed, averaged over the characteristics:

SNEAK-9A-1	RT1 and RT1 + RT2	5%
SNEAK-9A-2	RT1	6%
SNEAK-9A-2	RT2	3% <sup>+</sup> )
SNEAK-9A-2	RT1 + RT2	5%
SNEAK-9A-2	A	6%

---

<sup>+</sup>) A tilting effect of about + and -1% between the reactivity worths of the two control rod rings RT1 and RT2 calculated with the two cross-section sets was discovered; it is due to a minor difference in the condensation ways followed with both sets (condensation spectra for the absorbers RT1 and RT2).

From the 5-6%, 2% are explained by using 4 groups instead of 6.

The remaining 3-4% decrease of reactivity worths when going from MOXTOT to KFKINR is consistent with the cross-section modifications made, which correspond in general to a spectrum hardening /7/.

With KFKINR, isotope-dependent  $\chi$  values as recommended in /8/ were used; their effect on reactivity worths, with respect to the use of the standard ABBN  $\chi$  values, was calculated to be

$$+ 3 \pm 1\% \quad (\text{depending on the case}).$$

(The use of the standard values should have given lower C/E ratios.)

Indeed in the uranium core SNEAK-9A in which fission in  $^{235}\text{U}$  predominates, the new  $\chi$  values cause a spectrum softening.

#### 4.3 Comments on the C/E ratios (subcritical cases)

##### 4.3.1 Main results of SNEAK-9A

In SNEAK-9A-2, in which the absorber rods were inserted in the lower half of the core, one observes that the ratio C/E, for the four groups of measurements (RT1, RT2, RT1 + RT2, A) remains relatively constant versus insertion depth:

$$\begin{aligned} \text{C/E} &= 0.92 \pm 0.02 \text{ with KFKINR 4 groups (except 2 points)} \\ &0.96 \pm 0.02 \text{ with MOXTOT 6 groups (except 1 point)}. \end{aligned}$$

The C/E ratios averaged over the series of measurements are given in Table 4.3.

Table 4.3 Averaged C/E ratios of the control rod experiments in SNEAK-9A-1 and SNEAK-9A-2

Series	KFKINR 4 groups	MOXTOT 6 groups
SNEAK-9A-2 : RT1	0.92	0.98
SNEAK-9A-2 : RT2	0.92	0.95
SNEAK-9A-2 : RT1 + RT2	0.93	0.98
SNEAK-9A-2 : A	0.90	0.96
SNEAK-9A-2 : average values	0.92±0.02	0.97±0.02
SNEAK-9A-1 : RT1 <sup>+) )</sup>	0.94	0.99

<sup>+) )</sup> 2 first points not included.

In SNEAK-9A-1, in which the RT1 rods were inserted into the total core height, this tendency is also observed for the lower core half with however C/E ratios 2% higher. For small insertion depths, the C/E decreases significantly: the prediction becomes worse as one approaches the case "follower in" (see also the  $k_{eff}$  predictions compared for SNEAK-9A-1 and SNEAK-9A-2).

All the values C/E obtained in SNEAK-9A are presented versus rod insertion depth in Fig. 5 (SNEAK-9A-1) and Fig. 6 (SNEAK-9A-2).

From the SNEAK-6A and SNEAK-6D evaluations /9/, one extracts C/E values of 1.02 (6A) and 1.03 (6D) for the full insertion of a central rod  $\text{Na} - \text{B}_4\text{C}$ , calculated with NAPPMB or MOXTOT<sup>+</sup>) and with the same methods as here. For partial insertion depths of the central rod of 22.5, 45 and 67.5 cm in SNEAK-6A, the ratios obtained were respectively 0.87, 1.01 and 1.02.

These figures meet reasonably well those presently obtained; they are however systematically higher and the reasons for this discrepancy are still under investigation.

In SNEAK-9A-2, the comparison of the measured values for the characteristic (RT1 + RT2) with the sum of the value for both characteristics RT1 and RT2, indicates a shadowing effect which is zero or slightly negative (< -1%).

The calculations as well with KFKINR as with MOXTOT indicate on the contrary a positive shadowing effect; but its amplitude is also small (in general < 1%).

In SNEAK-9A-2, the simultaneous full insertion of all rods together (RT1 + RT2 + A) is measured 0.7% lower than the sum of the values measured independently. This negative shadowing effect is very well reproduced by calculations with KFKINR (-0.7%) and also with MOXTOT (-1.0%).

---

<sup>+</sup>) The deviation NAPPMB - MOXTOT was  $\leq$  1% relative.

#### 4.3.2 Note on transport results

Some cases were also calculated in the frame of the multigroup transport theory with 26 group cross-sections from the KFKINR set, using the Monte-Carlo program MOCA /10/. The current-weighted transport cross-section was employed. In each run 60 neutrons were followed over 120 generations; the results are given below together with their statistical accuracy, in terms of one standard deviation on the  $k_{eff}$  values obtained.

The MOCA results compare as follows with the corresponding KASY results:

Rod configuration in SNEAK-9A-2	$k_{eff}$ differences (in %)	$\Delta k$ reactivity changes
RT1/RT2/A (cm)	MOCA - KASY	ratio MOCA/KASY
40/40/0 (reference)	$1.0 \pm 0.2$	-
90/90/0	$1.1 \pm 0.2$	$0.96 \pm 0.10$
40/40/90	$1.3 \pm 0.2$	$0.93 \pm 0.06$
90/90/90	$1.1 \pm 0.2$	$0.97 \pm 0.04$

One observes transport effects, with respect to diffusion:

- of  $1.0 \pm 0.2\%$   $\Delta k$  on the  $k_{eff}$  value of the SNEAK-9A-2 core 40/40, which is in good agreement with the one obtained with other transport methods and reported in /9/;

- of  $-5 \pm 3\%$  relative in the average on the reactivity worths of control rod systems, which agree also well with the transport effects found in SNEAK-6A for the case of one central control rod /9/.

#### 4.4 Evaluation of the quasicritical measurements

##### 4.4.1 Characteristic curves of control rods

This paragraph gathers results of calculations relative to the reactivity worths measured in the cores (40/40) and (28/50) of SNEAK-9A-2 and corresponding to the displacement by  $\pm 9$  cm of a single RT1 rod and of two RT2 rods; see the description of the measurements in section 3.4.

The calculations were, as for the subcritical cases, performed using the KASY synthesis technique, with homogeneous 4 group KFKINR cross-sections. For the core 40/40 three trial functions, representative of 3 core slices, were employed, and for the core 28/50 four functions. The geometrical model for the calculations is a half core with symmetry conditions, which assumes 2 core elements more than actually realized (540 instead of 538), but this difference was assumed to have a negligible effect.

Table 4.4 gives the ratios of calculated over measured values of reactivity worths, for the case: core 40/40 (one RT1, two RT2), core 28/50 (one RT1). The results are also represented in curves on Fig. 7.

Table 4.4 C/E ratios for the characteristic curves of B<sub>4</sub>C control rods in SNEAK-9A-2 (measured values see Table 3.4)

Reference core configuration and rod insertion depth (cm)	C/E ratios	
	one RT1-rod pos. 17,18/16,17	two RT2-rods pos. 27,28/20,21 07,08/20,21
RT1/RT2 : 40/40		
31	0.88	0.90
34	0.87	0.90
37	0.87	0.92
40	reference	reference
43	0.87	0.88
46	0.87	0.91
49	0.87	0.90
RT1/RT2 : 28/50		
19	0.86	--
22	0.86	--
25	0.86	--
28	reference	--
31	0.84	--
34	0.84	--
37	0.84	--



When comparing with the evaluation of the subcritical measurements (section 4.2), one observes:

- for two RT2 in 40/40, a rather good agreement (C/E is about 0.90 against 0.92)
- for one RT1, in 40/40 or in 28/50, C/E values significantly lower here ( $\sim$  0.87 against 0.92).

This larger underestimate could be due to asymmetry (which introduced gradients): the reactivity of a single RT1 rod is worse predicted than the reactivity of the RT1 rod bank.

#### 4.4.2 Simulation of dummy assemblies for the SNR

Fig. 4 shows the core SNEAK-9A-2 with the nine radial positions successively occupied by the SNR dummy materials, simulated by four SNEAK elements containing either the bundle of  $B_4C$  pins already used for simulating the absorber rods ( $B_4C$  dummy), or a stack of normal sodium platelets (Na dummy).

In a basic core containing 538 elements the compensating rods RT1 and RT2 were respectively inserted to 26 cm ( $B_4C$  dummy) or 37 cm (Na dummy).

The reactivity worths, directly measured in  $\rho$ , were converted into  $\Delta k/k$  using the calculated value  $\beta_{eff} = 0.710\%$  (see also section 4.1.2).

The geometrical model used in the calculations is a half core with symmetry condition. It corresponds to 540 elements for the whole core, against 538 actually. The influence of those two additional elements on the reactivities of the dummies is neglected.

The KASY synthesis method is used with homogeneous cross-sections condensed from the KFKINR set into 4 groups.

The synthesis calculation was only made for the cases no dummy, and a dummy on position 1 and 9 respectively ( $B_4C$  and Na). Position 1 is central, position 9 is the most probable position for the SNR dummies. Each position for each type of dummy required to generate two appropriate trial functions (core with absorbers and with followers).

Table 4.5 gives together calculated and measured reactivity worths. Fig. 8 presents graphically the same comparison.

For the  $B_4C$  dummy the synthesis method gives the same C/E ratio for both positions 1 and 9 : 0.86. Such ratio is smaller than observed in preceding control rod evaluations.

For the Na dummy, the method gives respectively C/E = 1.03 (Pos. 1) and 1.02 (Pos. 9), i.e. an overestimate, as in general in previous evaluations, but smaller.

Subtracting the step fuel - Na from the step fuel -  $B_4C$  allows to consider the substitution Na -  $B_4C$ , i.e. the reactivity corresponding to the full insertion of an absorber. One observes the C/E ratio 0.80 for such reactivities on Pos. 1 and 9.

For comparison, the full insertion of the RT1 control rods in SNEAK-9A-1 was characterized by C/E = 0.94, and the full inser-

tion of the safety rods A in SNEAK-9A-2 by 0.90, for three different control rod configurations.

Table 4.5 Reactivity worths of  $B_4C$  and Na dummies, calculated and measured

Position of dummy (see Fig. 4)	Reactivity values in $10^{-4} \Delta k/k$		C/E ratio
	C, calculated	E, measured	
<u><math>B_4C</math> dummy</u>			
1	148.2	173.2	0.86
9	105.8	123.1	0.86
<u>Na dummy</u>			
1	41.7	40.6	1.03
9	32.4	31.9	1.02

The worse prediction obtained here might be associated with effects of mutual shielding between the different absorbers (control rods and diluent), but the measurements performed cannot separate and evidence these effects.

Two cores without dummies were realized as basic cores for the measurements; they contained the nine compensating rods all inserted to, respectively, 26 and 37 cm. Measured and calculated  $k_{eff}$  values compare as follows for these cores, and for the basic SNEAK-9A-2 core 40/40:

Core	E	C <sup>2)</sup>	C/E
26/26	1.0175 <sup>1)</sup>	1.0082	0.9909
37/37	1.0051	0.9977	0.9926
40/40	1.0004	0.9935	0.9931

One observes a trend to lower  $k_{eff}$  predictions with smaller insertion depths of control rods. This trend is coherent with the other SNEAK-9A evaluations, in particular with the smaller C/E ratio obtained for SNEAK-9A-1 (insertion depths : 0/0) of 0.9894 /1/. Also with the evaluation of the full characteristic RT1 measured in SNEAK-9A-1, which shows decreasing C/E ratios with decreasing insertion depths, see section 4.2.

---

1) The critical core actually realized was larger by 12 elements; the figure of 1.0175 for 538 elements was corrected for the core size effect.

2) Values corrected for a same core size of 538 elements.

## 5. Measurement of fission rate maps (power mapping)

### 5.1 General remarks

In the three core configurations of SNEAK-9A-2 with different insertion depths of the control rod banks RT1 and RT2 (core 1 : 40/40, core 2 : 28/50, and core 3 : 58/20) the power distribution was measured. To get a fairly good information of the three dimensional power map, axial power traverses were measured at 31 horizontal positions in each of the three configurations (see Fig. 9).

Three different techniques were used to achieve most reliable results:

- Measurement of axial traverses with fission chambers,
- Measurement of axial traverses by the activation of normal SNEAK fuel platelets,
- Measurement of radial and axial traverses by the activation of enriched uranium metal foils.

### 5.2 Fission chamber measurements

Fission chambers with  $^{238}\text{U}$  and  $^{235}\text{U}$  layers were moved through an axial channel of 12 mm diameter placed, in turn, at 31 representative positions in the core (see Fig. 9). The perturbation of the flux distribution by the fission chambers and channel was minimized

by fuelling the probe itself with enriched uranium and by using miniaturized electronics and cables. The fission chambers were calibrated in a reactor region with well-known fission rates. All data were recorded on a magnetic tape unit connected with a Honeywell DDP 124 on line computer /11/.

The fission rate distribution was measured with a standard deviation of 0.3% for  $^{235}\text{U}$  and 1% for  $^{238}\text{U}$ . As an example, the measured axial distribution of the total fission rate is shown in Fig. 10 for two different insertion depths of the adjacent RT1 control rod.

The results of the measurements used for the evaluation are the fission chamber results, summed over both isotopes  $^{235}\text{U}$  and  $^{238}\text{U}$  to give the total fission rates, after correction for the following effects:

- Drift of the electronic equipment

This longtime drift was probably due to radiation damages in the pre-amplifiers. A correction factor was obtained from repeated measurements of the fission product energy distribution spectra of the chambers. The correction factor was verified by repeating traverse measurements at identical positions at different times. Within a series of measurements this correction amounted up to 1%.

- Different setting of SNEAK shim rods

It was observed that the measured traverses were affected by the choice of the two SNEAK shim rods used for the reactivity compensation. From a theoretical study the assumption was made, that the power distribution  $P$  is perturbed according to

$$P' = P(1 + \beta r^2 \cos 2\beta),$$

where  $\beta$  is the azimuthal angle between the position of the measurement and the pair of SNEAK shim rods, and  $r$  is the distance of this position from the core axis.  $\beta$  was determined from several power maps at different shim rod insertions. The correction term in each position was < 1%.

- Perturbation caused by the measuring channel

The ratio of the fission rates in the channel to the fission rates in the cell fuel is not the same in both core zones R1 and R2. It was calculated using the program KAPER /12/ that the chamber results are to be increased in R2 by + 0.4% with respect to R1.

Table 5.1 gives for the three core configurations the total correction factors which were applied on the direct chamber results. For the first core (40/40), the three terms of the correction are also shown: the two first are predominant; there is often a certain compensation.

### 5.3 Activation measurements

The fission chamber measurements of the axial power distribution were independently checked by measuring the relative fission product  $\gamma$ -activity of the fuel from a few SNEAK elements. Platelets with low residual

Table 5.1 Corrections on fission chamber measurements

Designation of traverses	First core - 40/40			Second core 28/50	Third core 58/20	
	Partial corrections (in ‰ or 10 <sup>-3</sup> )			Total correction factor	Total correction factor	
	1.Drift	2.Effect of shim rods	3.Channel perturbation	Total correction factor	Total correction factor	
<u>Inner zone R1</u>						
18-10	+ 5.6	- 1.7	-	1.004	0.999	1.019
18-21	+ 0.7	- 1.7	-	0.999	1.000	1.019
18-18	+ 1.1	- 2.0	-	0.999	1.001	1.019
18-15	+ 1.4	- 3.0	-	0.998	1.013	1.019
18-13	+ 1.8	- 4.2	-	0.998	0.999	1.018
18-12	+ 2.1	- 4.9	-	0.997	0.999	1.017
18-23	+ 2.5	- 2.0	-	1.000	1.000	1.019
18-25	+ 2.8	- 2.6	-	1.000	1.000	1.018
18-28	+ 3.2	- 4.2	-	0.999	0.998	1.017
19-22	+ 3.5	- 1.5	-	1.002	1.003	1.021
19-23	+ 4.2	- 1.3	-	1.003	1.003	1.021
20-25	+ 5.0	- 0.7	-	1.004	1.004	1.023
20-24	+ 5.3	- 1.0	-	1.004	1.005	1.022
22-24	+ 6.0	+ 0.1	-	1.006	1.007	1.024
22-27	+ 6.4	- 0.3	-	1.006	1.007	1.024
21-26	+ 6.7	+ 1.0	-	1.008	1.002	1.025
23-25	+ 7.1	+ 1.1	-	1.008	1.009	1.025
24-26	+ 7.4	+ 0.1	-	1.008	1.008	1.025
<u>Outer zone R2</u>						
20- 8	+ 8.7	-10.6	+ 4.0	1.002	1.013	1.019
18- 8	+ 9.1	-10.2	+ 4.0	1.003	1.013	1.020
18- 9	+ 9.5	- 8.6	+ 4.0	1.005	1.015	1.021
18-10	+ 1.7	- 7.1	+ 4.0	0.999	1.016	1.023
18-11	- 2.6	- 5.9	+ 4.0	0.995	1.017	1.025
18-30	- 2.2	- 5.9	+ 4.0	0.996	1.017	1.025
24-30	- 1.9	- 4.9	+ 4.0	0.997	1.017	1.025
24-28	- 1.5	- 1.7	+ 4.0	1.001	1.020	1.028
25-27	- 1.1	- 1.2	+ 4.0	1.002	1.021	1.030
25-30	- 0.8	- 5.4	+ 4.0	0.998	1.016	1.026
26-30	- 0.4	- 5.5	+ 4.0	0.998	1.016	1.026
26-28	- 0.1	- 3.0	+ 4.0	1.001	1.018	1.029
26-25	+ 0.3	+ 0.4	+ 4.0	1.005	1.021	1.033



activity were substituted at selected positions within the core and after about 10-20 hours of irradiation at 500 W reactor power these platelets were unloaded and the relative  $\gamma$ -emission rates above discriminator settings at 430 keV, 580 keV and 890 keV were determined. Within counting statistics, all these energy regions yielded the same relative intensity distribution, indicating a negligible variation of fission product yield with neutron spectrum. In each configuration, three axial power traverses were obtained by this method within about  $\pm 1\%$  accuracy.

Finally, in the core mid-plane and at several positions near the axial core-blanket interface, uranium metal foils, with the same enrichment as the surrounding fuel, were irradiated and the total  $\gamma$ -activity of the fission products was determined. Supporting irradiations of depleted uranium foils were also carried out. The foil activation data yielded the power distribution in the core mid-plane and fission ratios  $\sigma_f^{28}/\sigma_f^{25}$  at several core positions.

#### 5.4 Comparison of the techniques

The activation data were, in general, in good agreement with the fission chamber measurements. Nevertheless, discrepancies up to 2% were revealed in the power measured close to the core-blanket interfaces and slightly larger discrepancies were found in the fission ratios  $\sigma_f^{28}/\sigma_f^{25}$ . These discrepancies have been attributed to changes in the flux fine structure, which cannot be detected by the fission chambers. However, they do not affect the power determinations inside the core regions.

Fig. 11 illustrates for three typical traverses in the first core (40/40) the general agreement between the three techniques of measurements.

For the comparison with the calculation therefore a data set, based on the fission chamber results was generated. After having applied the corrections mentioned in section 5.2, the experimental data were modified in two ways:

- a) Correction for values near the core-blanket boundary: the fission chamber results compared with activation results (foils and platelets) were too high in the external part of the traverses, due to streaming in the channel and/or due to the influence of the blanket. A set of empirical correction factors was deduced from the comparison with activation results: the correction is simply linear; it is zero for  $-30 \text{ cm} \leq Z \leq +30 \text{ cm}$  (from core mid-plane) and grows up to  $-1.5\%$  at  $Z = \pm 45 \text{ cm}$ ;
  
- b) A least squares fit of the measured points is performed with the code SENA-2 (developed by S. Pilate and G. Dziallas); it consists of placing each group of five neighbour points on a second order polynomial and assuming the central fitted result to be more accurate than the original value.

The accuracy for the points belonging to a single axial traverse was assumed to be 0.3% for one standard deviation. For the whole 3D power map a  $\sigma$ -value of about 1% was estimated. It is based on the checks of the radial dependence by independent techniques.

6. Calculation of the fission rate maps

6.1 Description of the calculations

6.1.1 Basic methods used

The 3D calculations were performed using the flux synthesis program KASY /2/, with KFKINR cross-sections /7/ condensed in four groups (scheme 4,6,10,26 according to the standard Russian structure). This implied, in fact, the use of the following sequence of computer programs:

1. NUSYS calculation of self-shielded cross-sections in 26 energy groups from the KFKINR set; condensation of cross-sections on the basis of zone spectra obtained in 1D and 2D diffusion calculations; substitution of the standard  $\nu$  values by new core average values, according to /8/;
2. DIXY 2D diffusion calculation, XY geometry, producing flux maps used as trial functions in the synthesis: group - and zone - independent values of  $B^2$  are used for the core slices /3/;
3. KASY see /2/, /3/, /9/ on the synthesis technique and its application. Fluxes are converged within  $10^{-3}$ ;

4. AUDI-3      this evaluation program /13/ yields local and integral rate distributions on the basis of the 3D KASY fluxes; used here for the total fission rate<sup>1)</sup>;
5. SENA-2      this program was especially written for an easy and systematic retrieval and evaluation of the experimental data at as many as  $3 \times 31 \times 91 \approx 8500$  points;
6. PLOTHL      some typical results are illustrated by plots /14/.

The basic series of calculations was made using a relatively broad mesh spacing. Each SNEAK element was subdivided into two mesh intervals in the X and Y directions of 2.72 cm each. This corresponds to  $38 \times 76$  points in the horizontal section, of which  $27 \times 53$  are in the core. Along Z, the calculation model contained as many points as the measurement, i.e., one each cm.

In the synthesis calculation of this basic series only two to three trial functions were used. These were flux distributions calculated for representative core slices.

---

1) Sum over the isotopes  $^{235}\text{U}$  and  $^{238}\text{U}$

The spatial distribution of total fission rate in the core is assumed to be also valid for the power density. This is not quite exact due to the effect of the gamma heat deposition rate on the total power density. This effect is investigated separately in several zero power assemblies. The term "power density" will often be employed here for "total fission rate".

In this study heterogeneous cross-sections for the fuel regions were calculated with the program ZERA /15/ in order to take into account the plate structure of the fuel cell.

The fuel compositions used were the pure cell compositions, which do not include any perturbation in the lattice such as SNEAK shim rods or rest cells.

#### 6.1.2 Normalization of fission rates

The results of calculations, which represent a full 3D map of fission rates  $R(x,y,z)$  in the core, were normalized to yield 1.0 for the mean along the 31 axial traverses selected for the experimental check:

$$\bar{R}_Z = \frac{1}{31} \sum_{i=1}^{31} \int_{\text{core height}, Z} R(z) dz \stackrel{!}{=} 1$$

The 31 traverse positions  $i$  were chosen in such a way that the mean value  $\bar{R}_Z$  approximates well the mean value over the whole core  $\bar{R}_C$ :

$$\bar{R}_C = \frac{1}{V_{\text{core}}} \int_{\text{core volume}, V} R(x,y,z) dx dy dz$$

A normalization  $\bar{R}_C = 1$  is especially practical for design calculations. For the first series of experiments a calculation yielded  $\bar{R}_C/\bar{R}_Z = 1.051$ , which is reasonably close to unity.

While the calculated results quoted in this section are given for a normalization  $\bar{R}_C = 1$ , all following comparisons between experiment (E) and calculation (C) refer to the normalization  $\bar{R}_Z = 1$ .

The results of calculations of the basic series are illustrated by Fig. 12 to Fig. 14. For one half of the SNEAK-9A-2 core cross-sections a series of isometric curves is plotted, showing the power axially integrated over the core height, for the cores 40/40 (Fig. 13), 28/50 (Fig. 13), and 58/20 (Fig. 14) (normalized to  $\bar{R}_C = 1$ ).

The maximum values of the axial integrals<sup>+)</sup>  are as follows:

Core	Maximum value of axial integrals	
	inner zone R1	outer zone R2
40/40	1.171	1.374
28/50	1.218	1.371
58/20	1.096	1.380

A comparison of the behaviour of the isopower curves for the three cores, shows that the influence of the control rod insertion is important in the R1 zone, but not in the R2 zone.

---

<sup>+)</sup>  Values at points, which do not coincide with positions of measured traverses. In the core 40/40, one has at the positions of the traverses:

18/20 (inner zone)	1.170
26/25 (outer zone)	1.297

Plots of the local power values in the core mid-plane of the reactor should show about the same behaviour but with a steeper radial gradient. For this core mid-plane, the maximum values of local power density are as follows (normalized to  $\bar{R}_C = 1$ ):

Core	Maximum values of local power in the core mid-plane	
	inner zone R1	outer zone R2
40/40	1.467	1.704
28/50	1.544	1.693
58/20	1.313	1.719

## 6.2 Basic results of the evaluation

### 6.2.1 $k_{eff}$ values

The  $k_{eff}$  values obtained with KASY in these power map calculations lead, when correcting for the core size model used and for the excess reactivities of the cores, to the following C/E ratios for the prediction of criticality (broad mesh):

Core	C/E
40/40	1.0019 <sup>+) </sup>
28/50	1.0017
58/20	1.0017

---

<sup>+)</sup>  1.0023 with a mesh spacing twice as fine in the core

These values differ from the corresponding ones quoted in /1, Table 3.3/, respectively<sup>+) 0.9981, 0.9978 and 0.9979, due to the input data (pure cell compositions), which are in this work adapted for the interpretation of power measurements. Nevertheless the small variations in C/E for the three cores indicate again that the  $k_{eff}$  prediction with diffusion is nearly independent of the control rod configuration.</sup>

#### 6.2.2 Power mapping evaluation for the first core (40/40)

The most important results of the evaluation for the first core (40/40) have been gathered in Table 6.1. For the sake of clearness the 31 traverses have been grouped in two series:

- a) a series East - West of 15 traverses along  $X = 18$  (see Fig. 9), direction perpendicular to the boundaries of the two core zones. Included are traverses near a RT1-rod and near the elements simulating a SNR safety rod (A-rod);
- b) a series NW - SE of the 17 remaining traverses. (This series includes traverses near an irregularly shaped part of the boundary between the two core zones and in the neighbourhood of RT1 and RT2 rods.)

---

<sup>+) Including the heterogeneity correction of  $0.0050 \delta k$ .</sup>



Table 6.1

Deviations (C-E)/E (in %) of axial integrals and local values for the power mapping in the first core (40/40) of SNEAK-9A-2

Position of traverses (see Fig. 9)	18-30	18-28	18-25	18-23	18-21	18-20	18-18	18-15	18-13	18-12	18-11	18-10	18-09	18-08	20-08
Note	Zone R2	Adjacent to rod "A"		Central pos. in zone R1				Near RT1 rod	Transition zone R1/ zone R2			Outer core boundary			
Deviations in % of axial integrals	-0.9	-1.0	-2.5	-1.5	-1.6	-1.4	-1.4	-0.7	0.7	2.1	-0.4	-0.1	0.8	1.6	2.1
Deviations in % of local values															
40	-0.4	2.0	0.9	0.8	0.5	0.4	3.0	4.1	2.6	4.0	0.6	1.3	2.2	3.1	3.8
30	0.7	0.3	-1.8	0.2	-0.5	-0.2	1.8	3.8	2.6	4.5	1.0	2.2	3.4	4.5	4.6
20	1.5	0.1	-1.6	-0.5	-1.0	-1.1	1.4	3.0	2.7	3.8	2.4	3.1	3.6	4.7	4.8
15	1.0	-0.2	-2.0	-1.1	-1.9	-1.6	1.0	2.7	2.6	3.8	2.0	2.5	3.3	4.1	5.0
10	0.7	0.1	-2.3	-1.1	-1.6	-1.4	0.5	2.3	2.0	3.8	1.4	1.9	3.0	4.2	3.6
5	-0.2	0.1	-1.7	-0.8	-1.1	-0.9	-0.1	0.7	1.5	3.0	0.6	0.9	1.8	2.6	2.6
0	-0.7	0.0	-1.2	-0.4	-0.2	-0.2	-0.7	-0.4	1.1	2.4	-0.4	0.1	0.5	1.4	1.5
- 5	-1.3	-0.7	-2.0	-0.9	-0.9	-0.7	-1.6	-1.1	0.4	1.8	-1.0	-0.5	0.1	0.9	1.2
-10	-0.8	-1.3	-1.7	-1.5	-1.1	-0.8	-2.3	-2.6	0.3	1.7	-1.4	-0.9	-0.3	0.7	1.2
-15	-1.4	-1.1	-2.5	-1.5	-1.7	-1.5	-2.7	-2.5	-0.5	0.9	-1.1	-1.2	-0.1	0.1	0.6
-20	-1.8	-1.6	-2.7	-2.4	-1.8	-1.9	-3.1	-3.0	-0.7	0.7	-1.6	-1.6	-0.8	-0.6	1.0
-30	-2.3	-2.6	-4.4	-2.9	-3.1	-3.1	-4.2	-4.0	-1.2	0.2	-2.4	-1.9	-1.4	-0.9	-0.1
-40	-4.5	-4.9	-6.1	-4.5	-4.2	-3.0	-5.7	-5.1	-2.3	-1.0	-3.4	-3.7	-2.6	-1.4	-0.9
Maximum of the traverses															
Pos. in measurement (cm)	-4.5	-9.0	-6.5	-10.0	-8.5	-7.5	-10.0	-9.5	-6.0	-5.5	-6.0	-7.5	-6.0	-4.0	-6.0
Shift by calcul. (cm)	0.0	2.5	0.0	2.5	1.0	0.0	1.5	1.5	0.0	0.0	1.0	2.5	1.5	0.0	2.0
Form factor (measured)	1.252	1.255	1.266	1.284	1.277	1.273	1.311	1.319	1.266	1.258	1.259	1.256	1.253	1.251	1.256
Deviat. of max. value	-1.3	-1.0	-2.2	-1.3	-1.0	-0.7	-2.2	-2.4	0.3	1.8	-1.2	-0.8	0.0	0.8	1.1
Deviat. of form factor	-0.4	0.0	0.3	0.2	0.6	0.7	-0.8	-1.7	-0.4	-0.3	-0.8	-0.7	-0.8	-0.8	-1.0

Table 6.1 continued

Position of traverses (see Fig. 9)	18-20	19-22	19-23	20-24	20-25	21-26	22-27	22-24	23-25	24-26	25-27	26-25	26-28	24-28	24-30	25-30	26-30	
Note	Most central pos.	Surrounding RT1-rod					In R1 near RT2 rod			Transition from R1 to R2		Maximum in R2		Near RT2-rod		Outer core boundary		
<u>Deviations in % of axial integrals</u>	-1.4	-1.5	-1.6	-1.3	-1.2	0.0	1.1	0.2	1.2	2.4	0.7	0.9	2.1	-0.4	1.7	2.2	3.5	
<u>Deviations in % of local values</u>																		
Ordinates in cm from core mid-plane	40	0.4	2.6	2.8	3.6	2.3	2.4	5.4	4.8	3.5	5.0	2.2	2.2	2.7	3.4	4.5	4.0	5.0
	30	-0.2	1.9	1.9	2.6	1.1	1.5	5.2	3.6	3.4	5.0	3.0	3.3	4.3	4.2	5.5	5.0	5.8
	20	-1.1	1.6	1.4	2.0	0.2	1.7	4.5	2.8	2.9	4.4	3.1	3.4	4.5	4.3	5.2	5.1	6.0
	15	-1.6	0.7	0.6	1.8	0.4	1.3	4.2	2.3	2.5	4.2	2.3	2.9	4.5	3.7	4.3	4.8	5.1
	10	-1.4	0.3	0.2	0.7	-0.2	1.0	3.2	1.9	2.7	3.9	2.6	2.7	3.6	2.7	3.9	4.2	4.9
	5	-0.9	-0.5	-0.7	0.1	-0.1	0.8	2.6	1.2	2.1	3.0	1.1	1.6	2.5	0.5	2.8	2.9	4.0
	0	-0.2	-0.9	-1.3	-0.7	-0.6	0.7	1.3	0.4	2.0	2.5	0.6	1.0	1.8	-1.0	1.5	2.4	3.1
	-5	-0.7	-1.5	-1.8	-1.9	-0.8	0.1	0.2	0.1	1.1	2.4	0.0	0.7	1.1	-1.9	0.7	1.6	2.4
	-10	-0.8	-2.0	-2.6	-2.4	-1.4	0.0	-0.6	-0.7	0.8	1.8	0.0	0.3	1.2	-2.1	-0.1	1.0	2.1
	-15	-1.5	-2.8	-2.6	-2.5	-1.4	-0.7	-0.6	-1.2	0.6	1.4	-0.5	-0.2	0.7	-2.2	0.2	1.0	1.8
	-20	-1.9	-3.1	-3.0	-3.2	-2.1	-0.8	-1.0	-2.1	0.4	1.4	-1.1	-0.4	0.9	-3.2	-0.4	0.1	1.6
	-30	-3.1	-4.1	-4.2	-4.5	-3.3	-1.9	-1.7	-2.3	-0.7	0.6	-1.0	-1.0	0.5	-3.4	-0.9	0.1	1.6
	-40	-3.8	-5.6	-5.8	-5.6	-4.4	-3.2	-3.2	-3.6	-1.6	-0.2	-2.1	-2.3	0.1	-4.5	-1.4	0.1	4.6
<u>Maximum of the traverses</u>																		
Pos. in measurement (cm)	-7.5	-8.5	-10.5	-9.0	-8.5	-8.0	-10.0	-10.0	-9.0	-8.0	-6.0	-7.0	-6.0	-7.0	-9.5	-7.0	-7.0	
Shift by calcul. (cm)	0.0	0.0	2.0	0.5	2.0	1.5	3.0	2.5	2.0	2.0	0.5	1.5	0.5	0.0	2.5	1.0	2.0	
Form factor (measured)	1.273	1.315	1.316	1.315	1.278	1.270	1.298	1.292	1.267	1.265	1.268	1.256	1.266	1.301	1.289	1.272	1.264	
Deviat. of max. value	-0.7	-2.2	-2.5	-2.4	-1.2	0.1	-0.3	-0.5	1.1	2.1	-0.2	0.4	0.9	-2.2	0.4	1.0	2.7	
Deviat. of form factor	0.7	-0.7	-0.9	-1.1	0.0	0.1	-0.8	-0.3	-0.1	-0.3	-0.9	-0.5	-1.2	-1.1	-1.3	-1.2	-0.8	

The relative deviations of the calculation from the measurement, (C-E)/E in %, are given for

- the fission rates integrated axially over the core height Z,  $\int R_i(z)dz$ ,
- the local fission rates at different axial heights (z=0 is the core mid-plane),
- the maximum fission rate:  $\text{Max}(R_i(z)) = R_i(z_0)$ .  
The  $z_0$ -position of the maximum in the measurement is indicated together with the shift of this position in the calculation,  $\Delta z_0$ .
- the form factor  $F_z$ , which is defined as

$$F_z = \frac{\text{Max}(R(z))}{\frac{1}{Z} \int_{\text{core height}} R(z)dz} ;$$

The measured form factor is also given.

The deviations of calculated from measured axial integrals are in general negative in the central zone R1 and positive in the outer zone R2, which reflects the trend of the calculations to give too flat a radial distribution; for the 18 traverses of the inner core zone R1 the average deviation is -0.4%, and for the 13 traverses of the outer core zone R2 it is +1.0%.

The maxima of the axial integrals are at position 18-20 in the inner core zone and at position 26-25 in the outer core zone. The calculation deviates there by -1.4% and +0.9%, respectively.

The highest deviations in R1 occur near a simulated safety rod (pos. 18-25 : -2.5%) and close to the R1/R2 boundary (18-12 : 2.1%, 24-26 : 2.4%); the vicinity of a RT1 rod is not worse predicted than a normal fuel position. In R2 they occur towards the outer core boundary (20-08 : 2.1%, 25-30 : 2.2%, 26-30 : 3.5%); the vicinity of a RT1 rod is not worse predicted than a normal fuel position.

Fig. 15 shows the relative deviations of the axial integrals written in the core-map.

Looking at the deviations of calculated from measured local power values there is a trend in the calculation to shift the axial traverses towards the upper core part, in which the positions of simulated control rods are filled with absorber materials. This indicates that the influence of the rod insertion on the power distribution is too weakly predicted. The deviations are therefore generally positive in the upper core part and negative in the lower part, they are more accentuated in the lower part (Fig. 11).

In order to make the picture clearer, curves of equal deviations of  $\pm 2$  and  $\pm 4\%$  have been drawn in Fig. 18 for the first series E-W of 15 traverses.

One sees that the deviations remain lower than  $\pm 2\%$  in a large part of the core, and that  $\pm 4\%$  is a maximum value for practically 95% of the core volume. Deviations of 5 and 6% exist rarely, except in the last 5 cm of the cores upper and lower part.

The position of the maximum of the traverses in the calculation in general shifted upwards by 2 cm. Its value is in general, pre-

dicted within  $\pm 2.5\%$ . The axial form factors are usually predicted within  $\pm 1.2\%$ .

Note that the axial form factor is about 1.26 in R1 as well as in R2, except near partially inserted control rods where it increases up to 1.32.

### 6.2.3 Power mapping evaluation for the two other cores (28/50, 58/20)

The results of evaluation for the two other cores (28/50 and 58/20) are presented with less details than for the first core (40/40). The complete results are available from the authors.

Table 6.2 shows for all 31 traverses, the deviations of calculated from measured axial integrals for the three cores. The general trend of the calculations to flatten the radial distribution is maintained. The deviations  $(C-E)/E$  are still generally negative in R1 and positive in R2. For the three cores and for each core zone the average deviations and the deviations at the positions of the power peaks are given:

Deviations $\frac{C-E}{E}$ (%)	40/40	28/50	58/20
R1 average (18 trav.)	- 0.4	- 0.5	- 0.2
R2 average (13 trav.)	+ 1.0	+ 1.2	+ 0.6
R1 peak (in pos. 18-20)	- 1.4	- 1.8	- 0.9
R2 peak (in pos. 26-25)	+ 0.9	+ 0.7	+ 0.5

Table 6.2 SNEAK-9A-2 power mapping. Deviations (C-E)/E in % of axial integrals. Comparison of the three cores.

Position of tra- verses (see Fig. 9)	First core (40/40)		Second core (28/50)	Third core (58/20)
		+) )		
<u>Zone R1</u>		+) )		
18-28	- 1.0	- 0.7	- 0.7	- 1.2
18-25	- 2.5	- 2.1	- 2.8	- 1.8
18-23	- 1.5	- 1.2	- 2.4	- 1.0
18-21	- 1.6	- 1.2	- 1.6	- 1.0
18-20	- 1.4	- 1.0	- 1.8	- 0.9
18-18	- 1.4	- 1.1	- 2.3	- 0.5
18-15	- 0.7	- 0.6	- 1.5	0.2
18-13	0.7	0.5	1.2	0.9
18-12	2.1	1.9	2.2	2.0
19-22	- 1.5	- 1.1	- 2.3	- 0.4
19-23	- 1.6	- 1.3	- 2.4	- 1.0
20-24	- 1.3	- 1.0	- 1.8	- 0.4
20-25	- 1.2	- 1.0	- 1.2	- 1.0
21-26	0.0	0.1	1.1	- 0.5
22-27	1.1	1.0	2.3	0.0
22-24	0.2	0.3	0.3	0.2
23-25	1.2	1.1	1.7	0.9
24-26	2.4	2.1	3.0	1.8
<u>Zone R2</u>				
18-30	- 0.9	- 0.8	0.0	- 0.8
18-11	- 0.4	- 0.6	- 0.4	- 0.6
18-10	- 0.1	- 0.3	- 0.1	0.2
18- 9	0.8	0.5	0.3	0.6
18- 8	1.6	1.3	1.1	0.9
20- 8	2.1	1.8	1.3	1.4
25-27	0.7	0.4	0.9	0.1
26-25	0.9	0.6	0.7	0.5
26-28	2.1	1.7	2.4	1.8
24-28	- 0.4	- 0.7	0.4	- 2.0
24-30	1.7	1.3	2.2	0.4
25-30	2.2	1.9	2.8	1.8
26-30	3.5	3.2	4.0	2.8

+) Using an additional blanket trial function

Fig. 16 (28/50) and Fig. 17 (58/20) show the relative deviations of the axial integrals.

It is to be noticed that in the neighbourhood of the control rods, the decrease of the axial integral values with increasing rod insertion depths (e.g. 28, 40, 58 cm) is underestimated by the calculation. This is probably related with the systematic underprediction of control rod worths.

The deviations of calculated from measured local power values are illustrated in Fig. 19 (28/50) and Fig. 20 (58/20). In a similar presentation as in Fig. 18 (40/40), the curves of iso-deviations  $\pm 2\%$  and  $\pm 4\%$  are drawn for the 15 traverses located along  $X = 18$ .

An examination of the three figures reveals that the prediction of the power map is slightly worse for the two last cores, for which the two groups of control rods RT1 and RT2 are inserted to different depths. The worst positions are not necessarily in the vicinity of control rods, but rather those placed in the highest radial gradients, e.g. near the core-blanket boundary.

The upwards shift of the axial position of the fission rate maximum is in general also observed for the two cores 28/50 and 58/20. The value of the maximum is still predicted within  $\pm 2.5\%$  and its relative value, i.e., the axial form factor within 1.2%.

In Table 6.3 the results of the evaluation are listed for three typical traverses: 18-20 (core center), 19-22 (R1 zone, near control rod), 26-25 (peak in outer zone R2).

Table 6.3 SNEAK-9A-2 power mapping. Deviations (C-E)/E in % of axial integrals and local values. Three typical traverses in the three cores (40/40, 28/50, 58/20)

Position of traverses (see Fig. 9)	18-20 (most central)			19-22 (R1, near RT1 rod)			26-25 (maximum in R2)		
	40/40	28/50	58/20	40/40	28/50	58/20	40/40	28/50	58/20
<u>Deviations in % of axial integrals</u>	- 1.4	- 1.8	- 0.9	- 1.5	- 2.3	- 0.4	0.9	0.7	0.5
<u>Deviations in % of local values</u>									
40	0.4	- 0.6	2.0	2.6	2.0	4.2	2.2	2.1	1.1
30	- 0.2	- 1.5	1.9	1.9	1.6	3.6	3.3	3.1	2.0
20	- 1.1	- 0.9	0.4	1.6	0.4	2.9	3.4	2.7	2.1
15	- 1.6	0.2	0.2	0.7	- 0.2	2.0	2.9	2.0	1.9
10	- 1.4	0.2	- 0.5	0.3	- 1.2	1.7	2.7	2.2	1.4
5	- 0.9	- 0.3	- 1.0	- 0.5	- 1.9	1.2	1.6	1.2	1.7
0	- 0.2	- 0.7	- 1.3	- 0.9	- 2.3	0.8	1.0	1.2	1.5
- 5	- 0.7	- 1.5	- 1.6	- 1.5	- 2.9	0.2	0.7	0.7	0.6
-10	- 0.8	- 1.9	- 2.0	- 2.0	- 3.3	- 0.6	0.3	0.2	0.7
-15	- 1.5	- 2.3	- 1.5	- 2.8	- 3.6	- 1.3	- 0.2	0.2	0.1
-20	- 1.9	- 2.8	- 1.0	- 3.1	- 3.9	- 2.6	- 0.4	- 0.2	- 0.6
-30	- 3.1	- 3.3	- 1.5	- 4.1	- 4.5	- 4.5	- 2.3	- 2.0	- 2.4
-40	- 3.8	- 4.7	- 3.8	- 5.6	- 6.5	- 5.6	- 2.3	- 2.0	- 2.4
<u>Maximum of the traverses</u>									
Pos. in measurement (cm)	- 7.5	- 6.0	-10.0	- 8.5	- 6.5	-18.0	- 7.0	- 6.0	- 4.5
Shift by calcul. (cm)	0.0	2.5	- 3.0	0.0	1.5	2.5	1.5	1.0	1.0
Form factor (measured)	1.273	1.270	1.229	1.315	1.292	1.246	1.256	1.246	1.248
Deviat. of max. value	- 0.7	- 1.6	- 2.0	- 2.2	- 2.9	- 1.8	0.4	0.5	0.7
Deviat. of form factor	0.7	0.2	- 1.1	- 0.7	- 0.6	- 1.4	- 0.5	- 0.2	0.2



6.3 Check of methods

6.3.1 Effect of mesh spacing, of blanket trial functions and of condensation

For the first core (40/40), the basic calculation was repeated using a fine mesh spacing in the core region: 1.36 cm along X and Y against 2.72 cm (64 x 128 points in the horizontal section instead of 38 x 76). Along Z the mesh spacing was not varied (1 cm in the core, as in the measurements).

The influence of the mesh size on the deviations,  $(C-E)/E$ , for the axial integrals is a change by about  $\pm 0.1\%$  for 20 of the 31 traverses. It increases up to 0.4% for the rest (see Table 6.4).

Table 6.4 Influence of the mesh spacing on to the axial power integrals

Traverses	Deviations $(C-E)/E$ in % of axial integrals when the mesh spacing effect exceeds 0.2%	
	Broad mesh	Fine mesh
R1 - 18-12	2.0	2.3
R2 - 20- 8	2.1	2.5
18- 8	1.6	2.0
18- 9	0.8	1.1
18-10	- 0.1	0.2
18-11	- 0.4	- 0.1
18-30	- 0.9	- 1.2

The mesh spacing effect is the highest in the regions of high radial gradients, but even there it is so small that it can be neglected in the comparison of calculation and experiment.

The comparison of the results obtained with and without a blanket trial function for the first core (40/40) illuminates the influence of adding a blanket trial function to the core trial functions used for the synthesis. The deviations of calculated from measured axial integrals are systematically but moderately reduced, as can be seen in Table 6.2.

This systematic effect indicates an improvement of the prediction of the radial dependency of the power map due to the additional trial function.

The effect on the local values is less obvious. Table 6.5 shows this effect for the three typical traverses 18-20, 19-22 and 26-25. One observes that the blanket trial function does not improve systematically all local values.

An earlier fundamental study by C. Hoenraet and S. Pilate on the use of blanket trial functions had already indicated that the additional expense made, results only in minor improvements for the core region but in major improvements in the axial blanket regions.

The effect of cross-sections condensation was investigated with 2D calculations and was still checked in three dimensions. The basic 4 group condensation scheme (4,6,10,26) was compared with a 6 group scheme (4,6,8,10,12,26), with a 12 group scheme (2,3,.....,10,12,15,26) and with 26 groups (in 2D only).

Table 6.5

Effect of blanket trial functions.  
First core (40/40) - Three typical traverses

Position of traverses (see Fig. 9)	18-20		19-22		26-25	
	A <sup>+</sup> )	B <sup>++)</sup>	A <sup>+</sup> )	B <sup>++)</sup>	A <sup>+</sup> )	B <sup>++)</sup>
Deviations in % of <u>axial integrals</u>	- 1.4	- 1.0	- 1.5	- 1.1	0.9	0.6
Deviations in % of <u>local values</u>						
Ordinates in cm from core mid-plane						
40	0.4	2.2	2.6	4.2	2.2	1.6
30	- 0.2	1.0	1.9	3.0	3.3	2.8
20	- 1.1	- 0.2	1.6	2.4	3.4	2.9
15	- 1.6	- 0.7	0.7	1.3	2.9	2.3
10	- 1.4	- 0.7	0.3	0.8	2.7	2.2
5	- 0.9	- 0.7	- 0.5	- 0.3	1.6	1.3
0	- 0.2	- 0.4	- 0.9	- 1.0	1.0	1.0
- 5	- 0.7	- 1.0	- 1.5	- 1.7	0.7	0.6
-10	- 0.8	- 1.1	- 2.0	- 2.2	0.3	0.3
-15	- 1.5	- 1.7	- 2.8	- 3.0	- 0.2	- 0.3
-20	- 1.9	- 2.0	- 3.1	- 3.1	- 0.4	- 0.5
-30	- 3.1	- 3.0	- 4.1	- 4.0	- 1.0	- 1.1
-40	- 3.8	- 3.2	- 5.6	- 5.0	- 2.3	- 2.5
<u>Maximum of the traverses</u>						
Pos. in measurement (cm)	- 7.5		- 8.5		- 7.0	
Shift by calcul. (cm)	0.0	0.0	0.0	0.0	1.5	1.5
Form factor (measured)	1.273		1.315		1.256	
Deviat. of max. value	- 0.7	- 1.0	- 2.2	- 2.4	0.4	0.3
Deviat. of form factor	0.7	0.0	- 0.7	- 1.3	- 0.5	- 0.3

+ ) Only core trial functions used (reference calculation)

++ ) One additional blanket trial function used

Table 6.6 shows the effect of condensation on local values for a few traverses. One observes a maximum effect of 2 to 3% in the neighbourhood of control rods and near the outer core boundary; the positive sign in the upper part of the core and the negative sign in the lower part mean that the axial flux tilting in 4 groups is somewhat reduced when using 6 or 12 groups.

Table 6.6      Effect of condensation in the first core (40/40)  
(Deviations of local values against values calculated with 12 groups in %)

Position of the traverses		18-30	18-28	18-21	18-18	18-15	18-11	18-08
		Distance from core-midplane (cm)						
4 groups	35	0.1	0.1	0.9	2.6	2.9	1.1	1.6
	25	- 0.1	0.2	0.8	2.4	2.7	0.9	1.5
	15	- 0.2	0.0	0.6	2.3	2.4	0.6	0.9
	-15	0.2	0.3	- 0.1	- 1.1	- 1.2	- 0.3	- 1.4
	-25	0.1	0.2	- 0.4	- 1.4	- 1.5	- 0.5	- 1.6
	-35	0.1	- 0.5	- 1.0	- 2.0	- 2.2	- 0.9	- 2.0
6 groups	35	0.3	0.3	0.4	0.5	0.5	0.0	0.5
	25	0.2	0.4	0.4	0.5	0.5	0.0	0.5
	15	0.2	0.3	0.3	0.4	0.4	- 0.1	0.3
	-15	- 0.1	0.0	- 0.1	- 0.2	- 0.1	0.1	- 0.8
	-25	- 0.2	- 0.1	- 0.2	- 0.3	- 0.2	0.0	- 0.9
	-35	- 0.3	- 0.4	- 0.5	- 0.5	- 0.5	0.0	- 1.2

The condensations does not influence significantly the axial form factors.

The effect of condensation on the axial integrals (not given in Table 6.6) is in relation with the too flat radial power distribution obtained by 4 group calculations: part (but not all) of this radial tilting effect is removed when using 6 or 12 groups instead of 4.

### 6.3.2 Notes on cross-section set influence and transport results

The calculations for the first core 40/40, basically made with the KFKINR cross-section set, have been repeated using MOXTOT cross-sections. The differences in the calculated power maps are in general small, specially for the axial integrals and the form factors. One observes that the overestimate of the calculated local values with respect to experiment in the upper part of the core is larger with KFKINR than with MOXTOT, which is probably in relation with the smaller control rod worths calculated with KFKINR.

In a 2D cylindrical model representing a central control rod in a simplified SNEAK-9A core, transport ( $S_6$ ) and diffusion calculations have been compared. The examination of the axial traverses obtained for a partial insertion of the rod has showed that the axial flux tilting observed with diffusion should be significantly reduced with transport.

References

- /1/ M. Pinter  
Physics Investigations of Sodium Cooled Fast Reactors  
SNEAK-Assembly 9A  
KFK-2028 (July 1974)
- /2/ G. Buckel  
Approximation der stationären dreidimensionalen Mehrgruppen-  
Neutronen-Diffusionsgleichung durch ein Syntheseverfahren mit  
dem Karlsruher Syntheseprogramm KASY  
KFK-1349 (Juni 1971)
- /3/ S. Pilate et al.  
A three-dimensional synthesis method tested and applied in  
fast breeders  
KFK-1345 (August 1971)
- /4/ G.R. Keepin  
Physics of nuclear kinetics  
Addison-Wesley Publishing Company, Inc. 1965
- /5/ L. Tomlinson  
Delayed Neutrons from Fission  
A Compilation and Evaluation of Experimental Data  
AERE-R 6993 (February 1972)

- /6/ F. Helm et al.  
Control rod measurements in an uranium fueled mock-up of  
the fast breeder prototype SNR  
IAEA Conference Tokyo, October 1973
- /7/ E. Kiefhaber  
The KFKINR Set of Group Constants  
KFK-1572 (March 1972)
- /8/ E. Kiefhaber, D. Thiem  
The influence of fission neutron spectra on integral nuclear  
quantities of fast reactors  
KFK-1561 (March 1972)
- /9/ S. Pilate, F. Plum  
Control rod experiments in SNEAK-Assembly 6  
KFK-1633 (July 1972)
- /10/ J. Lieberoth  
A Monte Carlo Technique to Solve the Static Eigenvalue  
Problem of the Boltzmann Transport Equations  
Nucleonics 11, Vol. 5, pp. 213-219 (1968)
- /11/ R. Böhme  
Messung des Einflusses von Kontrollstäben auf die Leistungs-  
verteilung in der SNR-300-Nachbildung SNEAK-9A-2 - Spaltkam-  
mertraversen -  
KFK-1273/1, PSB 1. Vierteljahresbericht 1973, S. 121-15

- /12/ P.E. Mc Grath, E.A. Fischer  
Calculation of Heterogeneous Fluxes, Reaction Rates and Reactivity Worths in the Plate Structure of Zero Power Fast Critical Assemblies  
KFK-1557 (March 1972)
- /13/ G. Willerding et al.  
AUDI-3 Ein Rechenprogramm zur Auswertung von Neutronenflußverteilungen aus Multigruppendiffusionsrechnungen in drei Raumdimensionen  
KFK-report in preparation
- /14/ U. Schumann  
PLOTHL, ein FORTRAN IV Unterprogramm zur Darstellung von Funktionen von zwei unabhängigen Variablen durch ihre Höhenlinien auf einem Plotter  
KFK-1486 (Oktober 1971)
- /15/ D. Wintzer  
Zur Berechnung von Heterogenitätseffekten in periodischen Zellstrukturen thermischer und schneller Kernreaktoren  
KFK-743 (1969)
- /16/ F. Helm et al.  
Physics Investigations of Sodium Cooled Fast Reactors SNEAK-Assembly 2  
KFK-1399 (June 1971)
- /17/ M. Billaux et al.  
Control Rod Optimization for the SNR-300  
IAEA Conference Tokyo, October 1973



Appendix A

Determination of the correction factors for the  
subcritical source multiplication technique

We start with the neutron balance equation in the point reactor model

$$-\Sigma_a \phi + \nu \Sigma_f \phi + S = 0, \quad (1)$$

assuming that the system is subcritical and contains an arbitrary neutron source  $S$ . Introducing the multiplication factor  $k = \nu \Sigma_f / \Sigma_a$  and the reactivity  $\rho$ , we obtain

$$\beta \cdot \rho \equiv \frac{1 - k}{k} = \frac{S}{\nu \Sigma_f \phi}. \quad (2)$$

The neutron flux  $\phi$  can be related to the counting rate  $Z$  of a neutron detector with the efficiency  $W$  in terms of counts per fission, and we obtain the well known relation

$$\beta \cdot \rho = \frac{S \cdot W}{Z}. \quad (3)$$

The proportionality factor between  $\rho$  and  $1/Z$  is normally obtained by a calibration with a known reactivity  $\rho_0$  and a measured counting rate  $Z_0$ . An arbitrary reactivity state is then given by

$$\rho = \rho_0 \cdot \frac{Z_0}{Z} \quad (4)$$

because  $W$  and  $S$  are constant in the point reactor model.

But regarding that the profiles of the real and adjoint fluxes may alter by changing the reactivity for instance by inserting a control rod, this is no longer true. We therefore transform the Eq. (2) to a more general, space dependent form

$$\beta \cdot \rho = \frac{\int S(x) \phi^+(x) dx}{\int v \Sigma_f \phi(x) \phi^+(x) dx} \quad (5)$$

Using again the relation of Eq. (3), we obtain the following expressions for the detector efficiency  $W$  and the effective source strength  $S_{\text{eff}}$

$$W = \frac{\int_{\text{detector}} \Sigma_d \phi(x) dx}{\int_{\text{reactor}} v \Sigma_f \phi(x) dx} \quad (6)$$

$$S_{\text{eff}} = \frac{\int_{\text{source}} S(x)\phi^+(x)dx \cdot \int_{\text{reactor}} \nu\Sigma_f\phi(x)dx}{\int_{\text{reactor}} \nu\Sigma_f\phi(x)\phi^+(x)dx} \quad (7)$$



The calibration is again performed with a known reactivity state  $\rho_0$  and the values  $Z_0$ ,  $S_{\text{eff},0}$ , and  $W_0$  belonging to it. Each sub-critical state is then given by

$$\rho = \rho_0 \cdot \frac{Z_0}{Z} \cdot F \quad (8)$$

with the correction factor

$$F = \frac{S_{\text{eff}} \cdot W}{S_{\text{eff},0} \cdot W_0} \quad (9)$$

which is to be calculated for each case separately.

-  CONTROL ROD
-  SECONDARY SHUT DOWN ROD

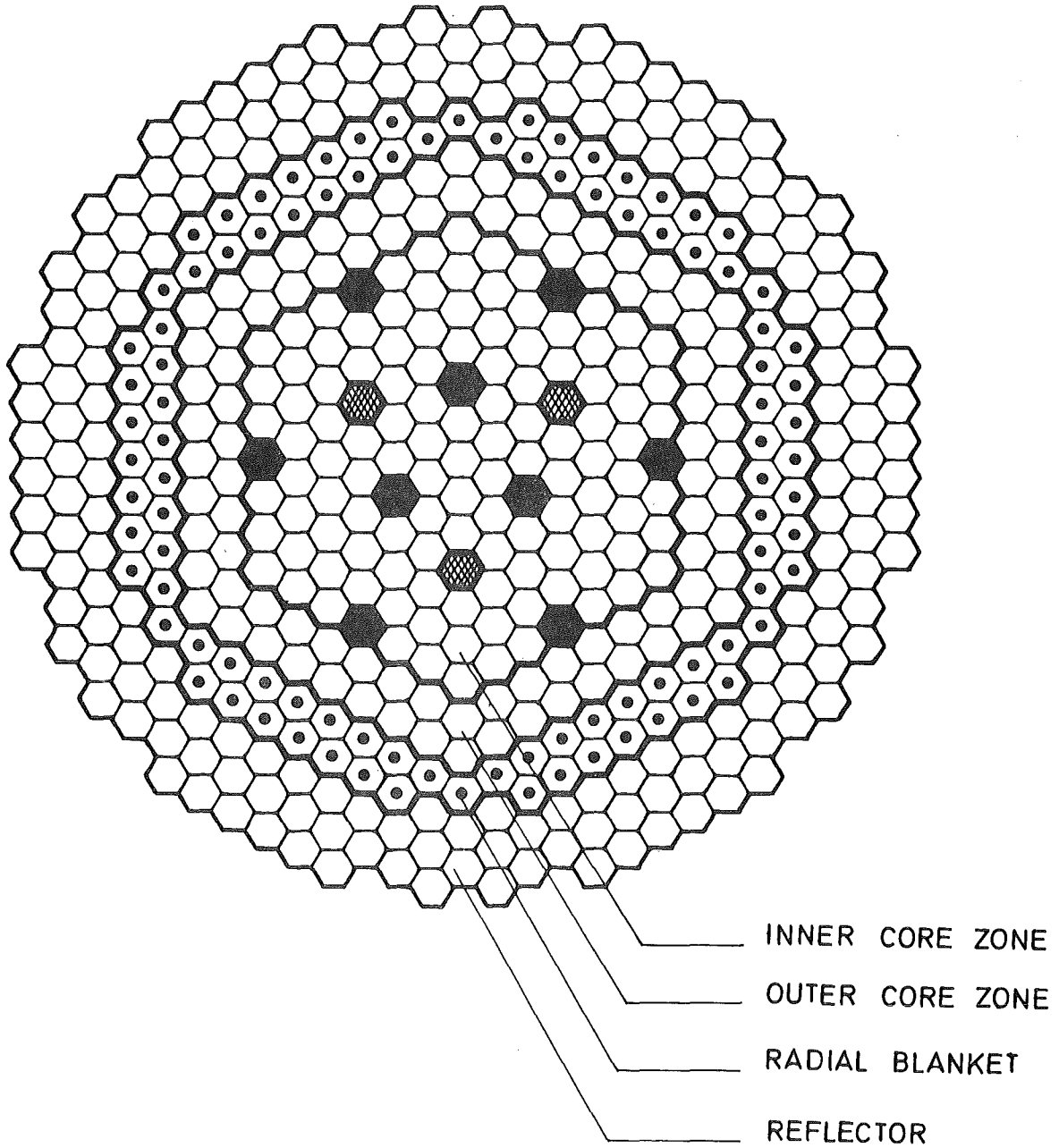


FIG. 1  
SNR -300 MARK -1A CORE

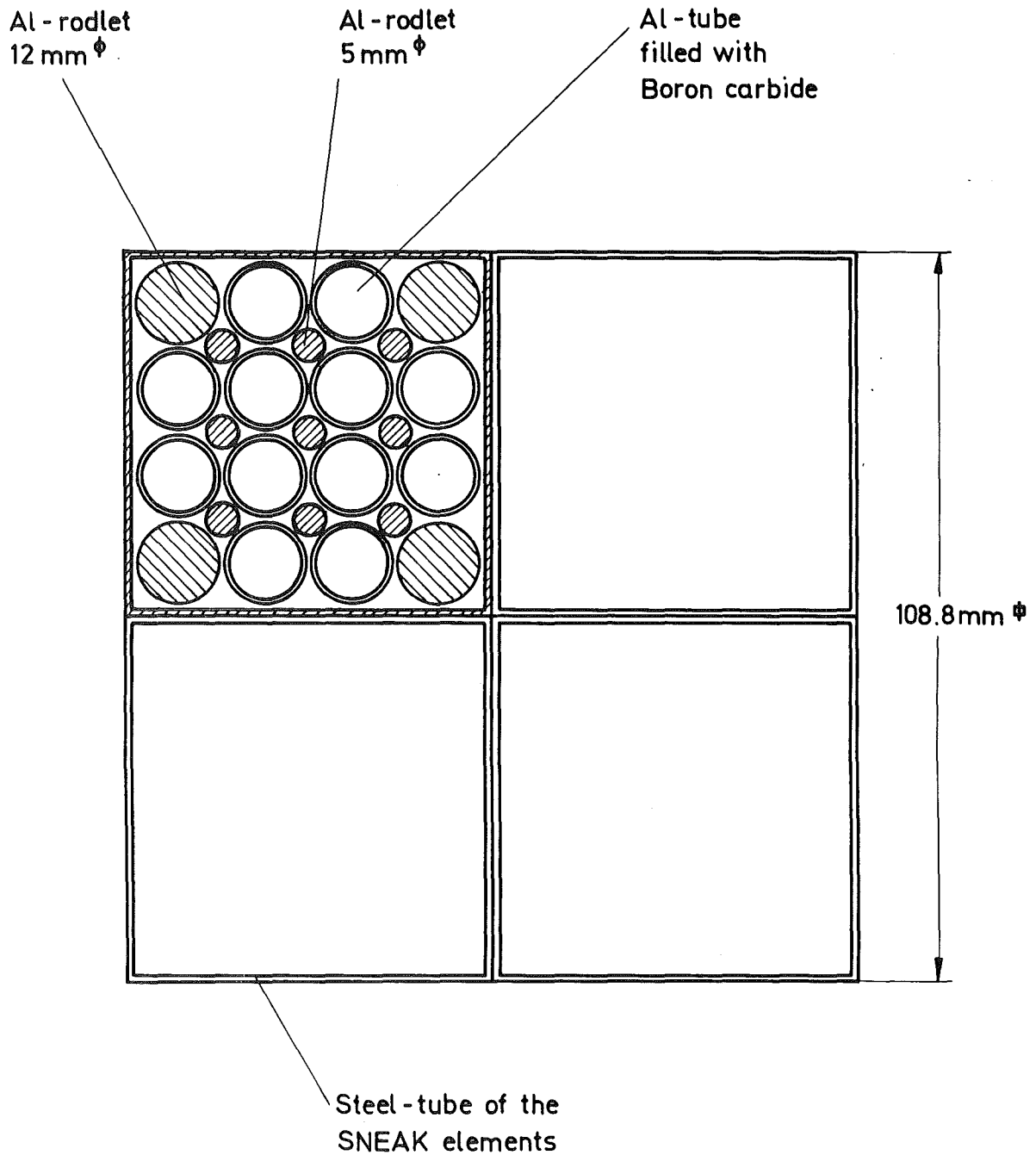
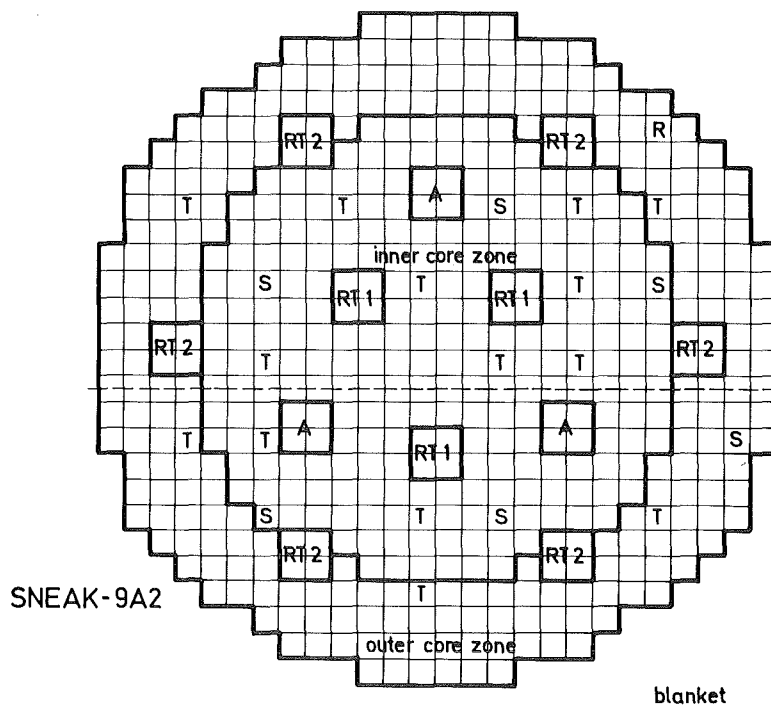
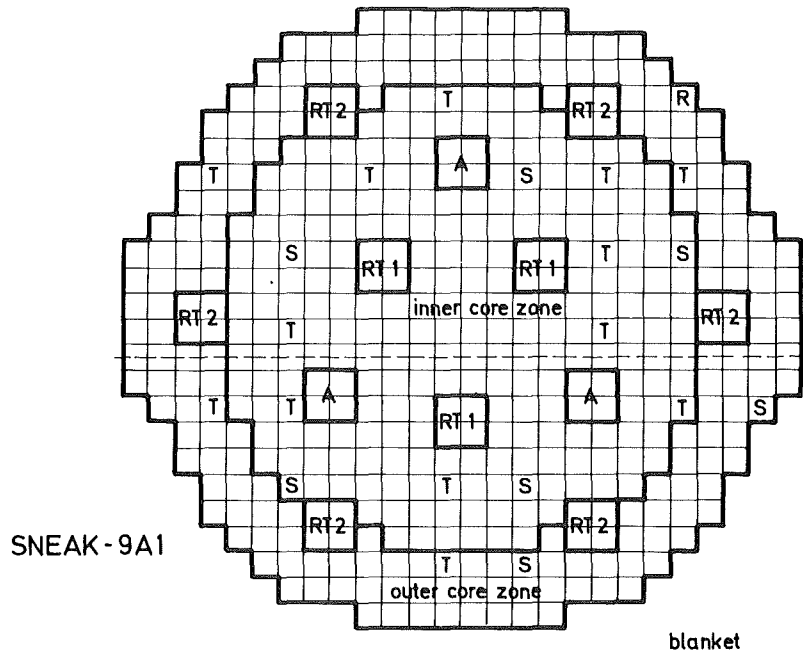


Fig. 2 Cross Section through a SNR-Control Rod, simulated by 4 SNEAK-Elements



- S = safety rod
- T = shim rod
- R = regulating rod
- A = simulated SNR safety rod
- RT1, RT2 = simulated SNR regulating rod

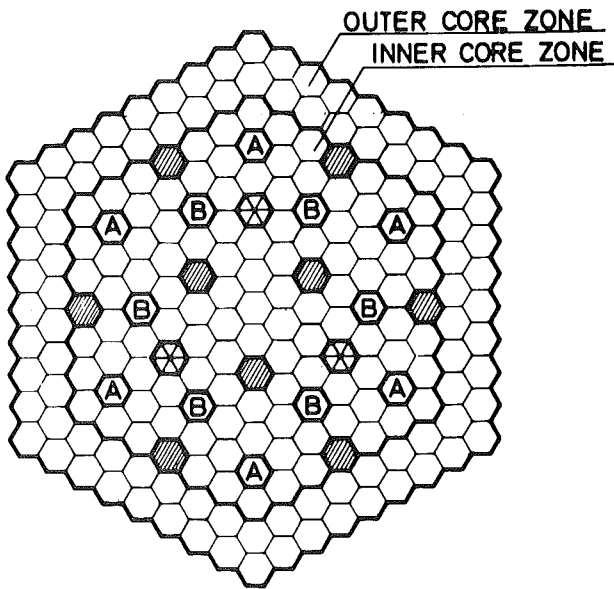
Fig.3 Horizontal Cross Sections of the Critical Configurations of SNEAK-9A1 and -9A2

▨ CONTROL ROD

⊗ SHUT DOWN ROD

Ⓐ B<sub>4</sub>C DILUENT

Ⓑ Na DILUENT



▨ CONTROL ROD

⊗ SHUT DOWN ROD

Ⓘ B<sub>4</sub>C OR Na DILUENT

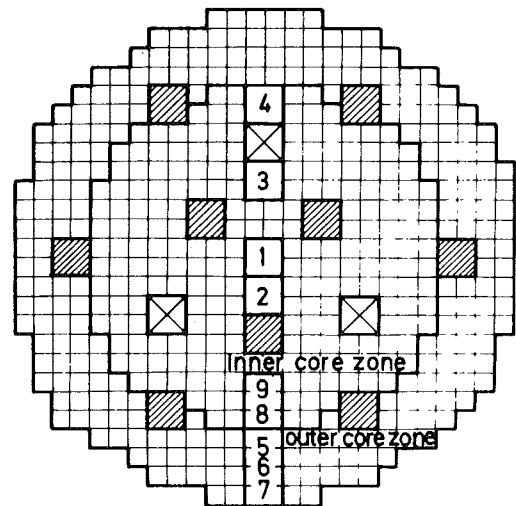


Fig.4 Core Layout of SNR-300 (left) and of SNEAK-9A2 (right)

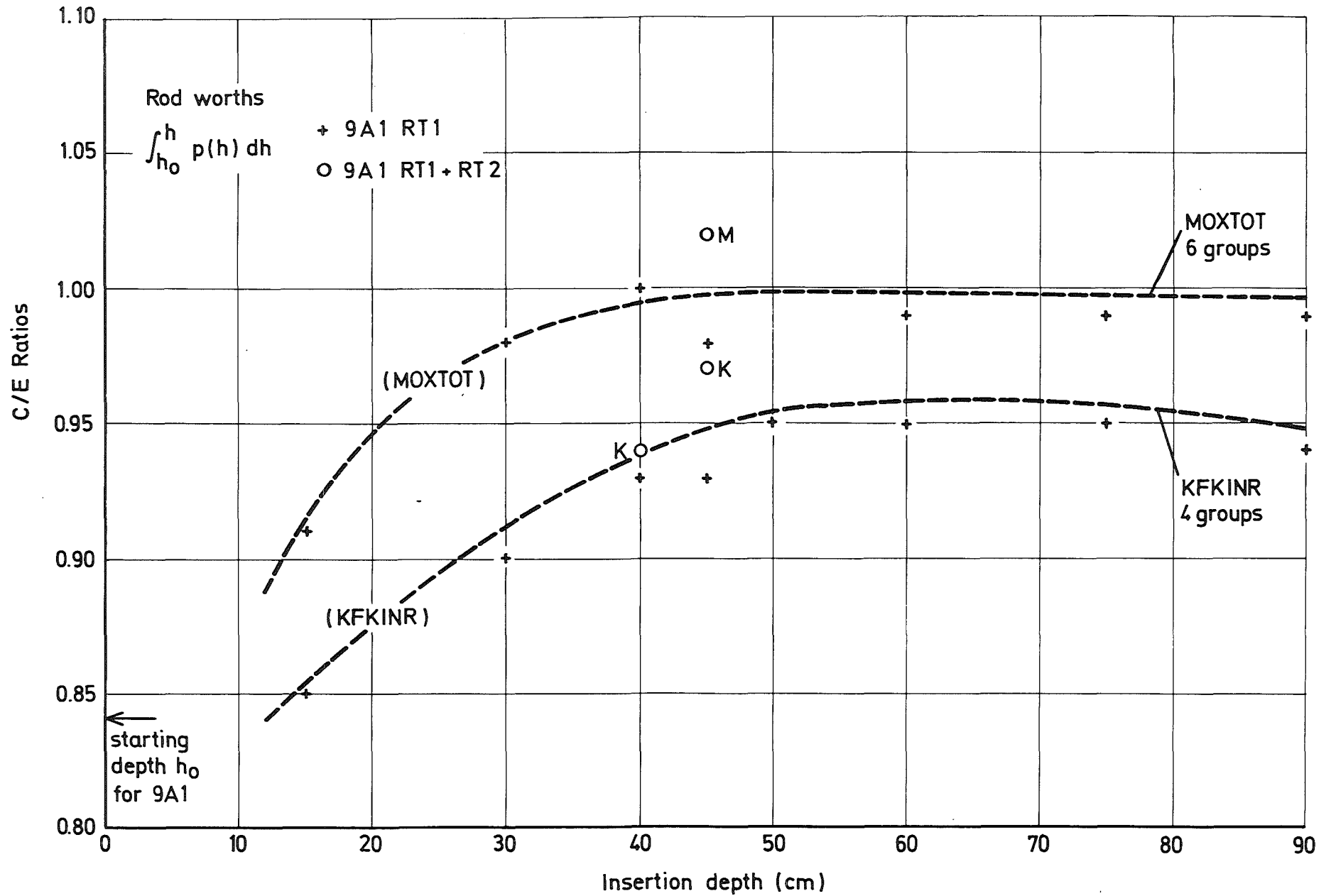


Fig.5 Subcritical Measurements in SNEAK - 9A 1  
 Calculation - over - Experiment Ratio versus Rod Insertion Depth



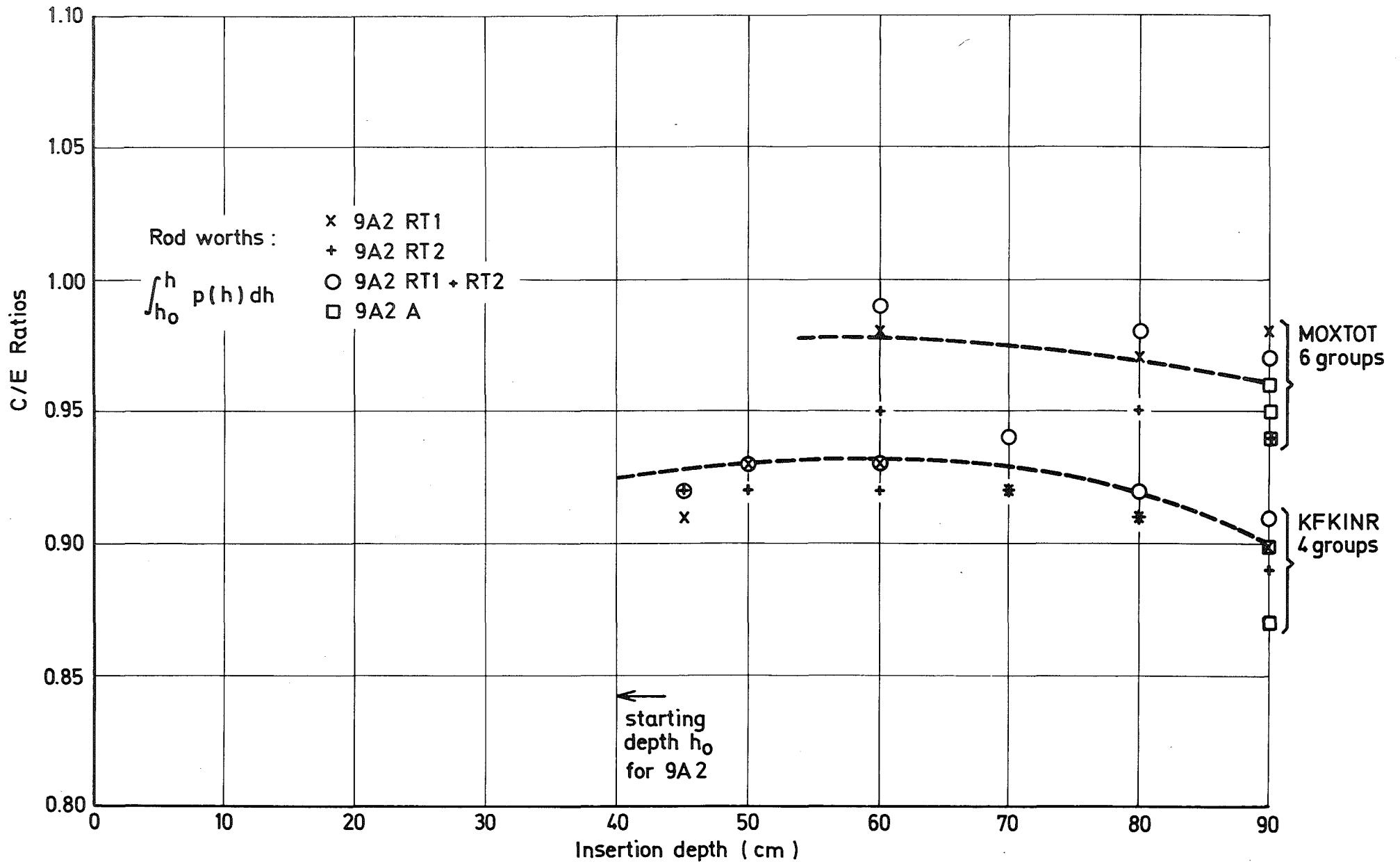


Fig. 6 Subcritical Measurements in SNEAK-9A2  
 Calculation - over - Experiment Ratio versus Rod Insertion Depth

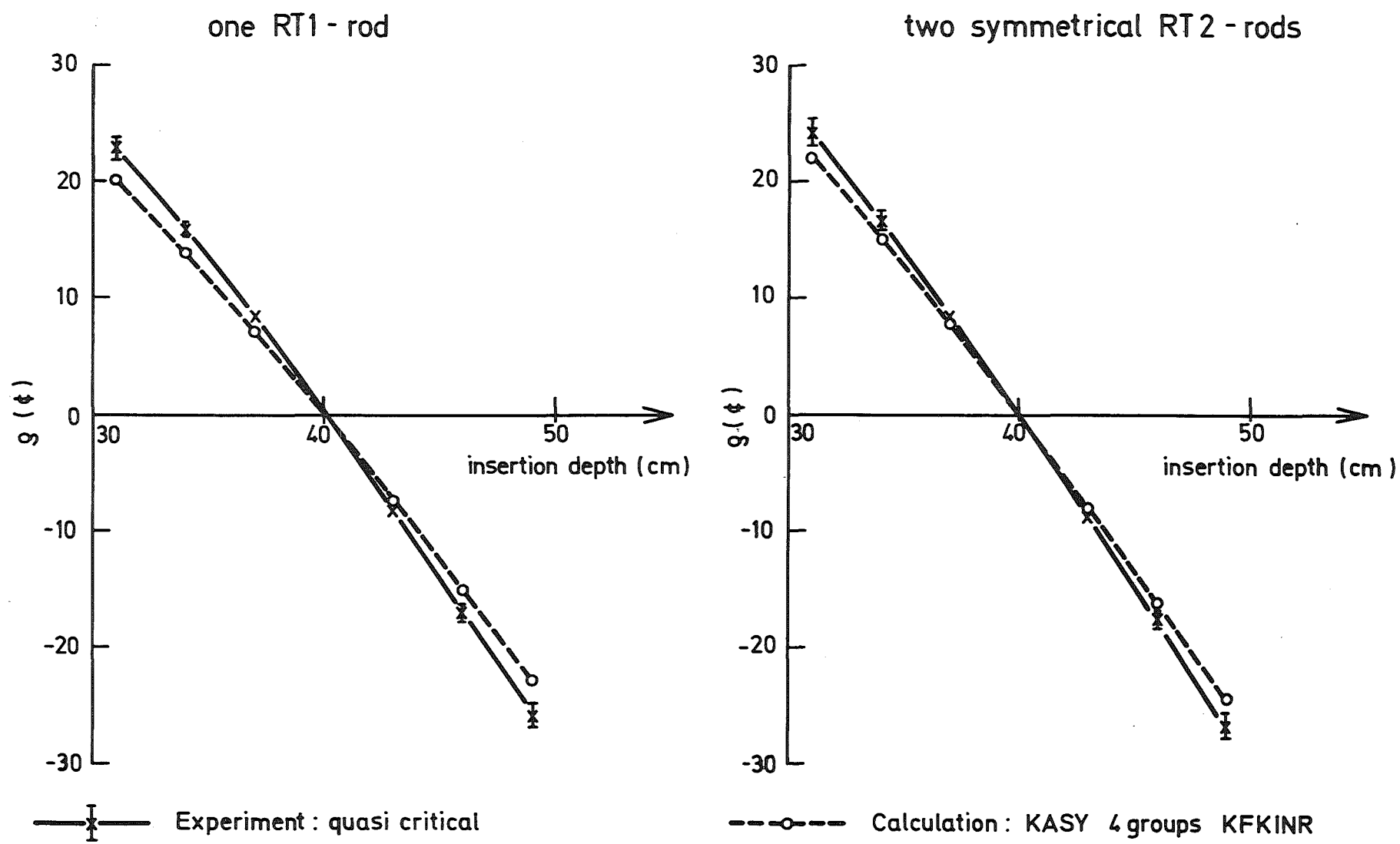


Fig.7 Comparison of Calculation and Experiment for small Changes of the Control Rod Insertion Depth

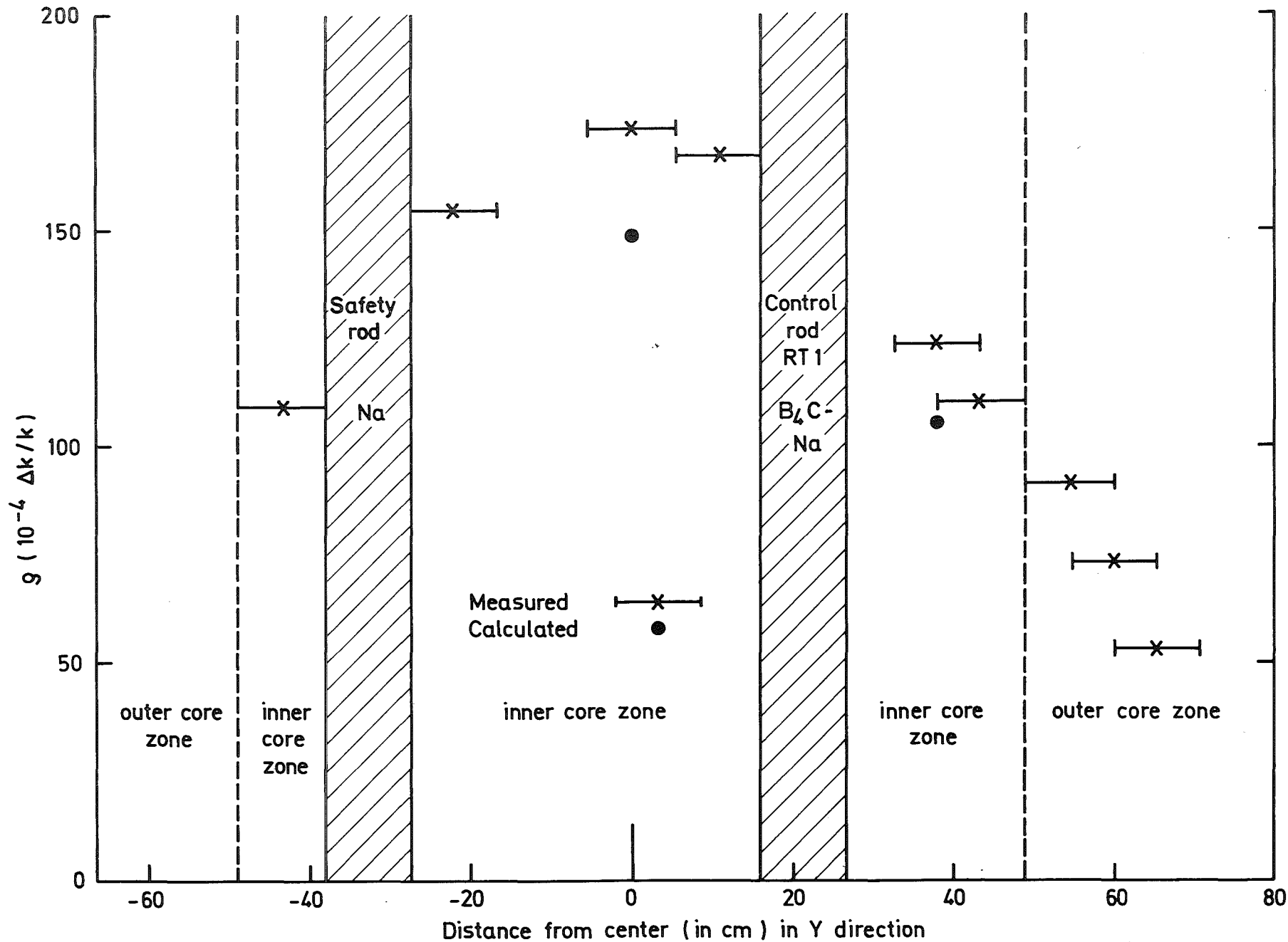
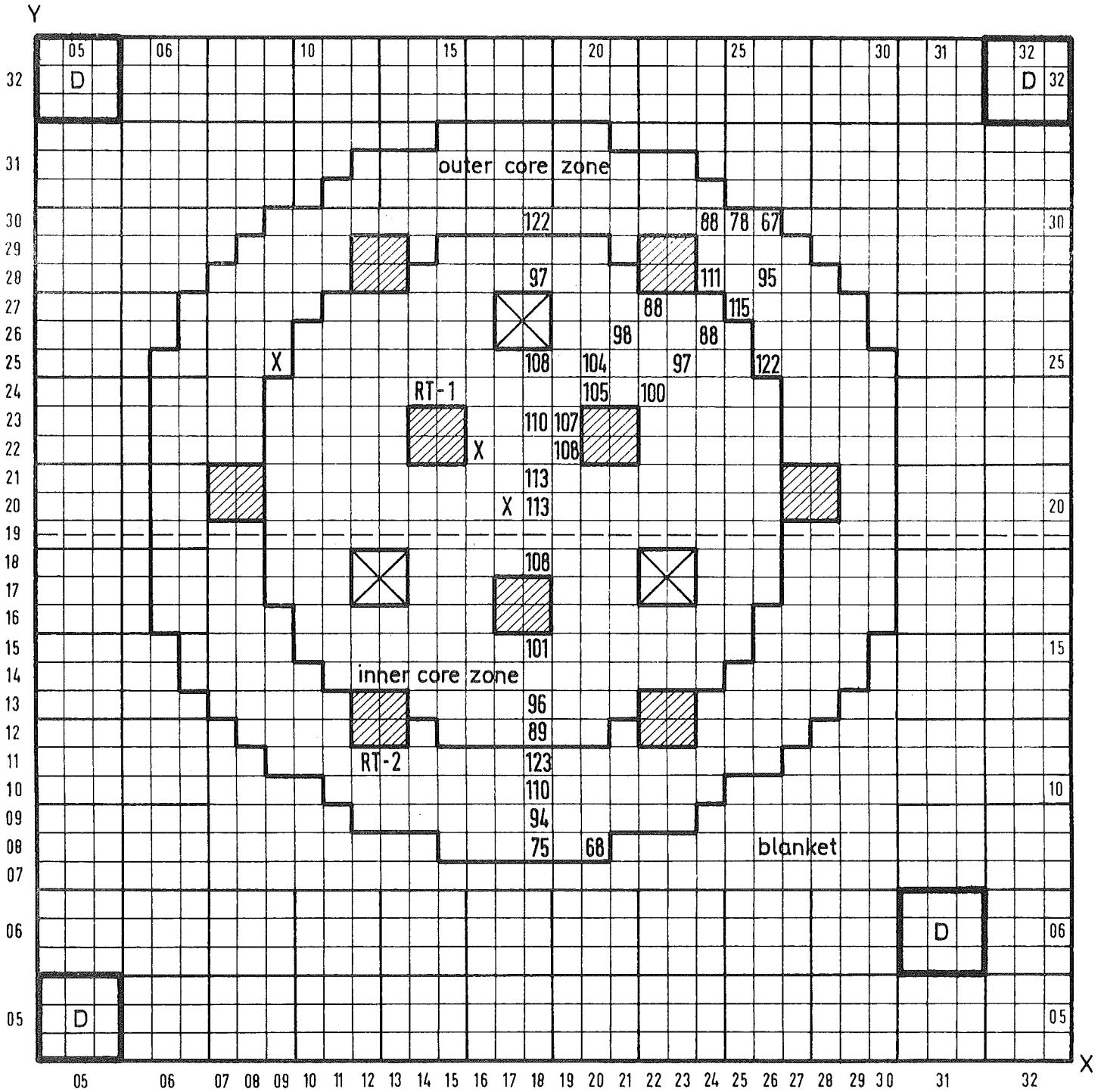

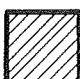



Fig. 8 SNEAK-9A, B<sub>4</sub>C Diluent Reactivity Worth on 9 Different Positions



-  Neutron detector
-  Simulated SNR control rod (RT1 and RT2)
-  Simulated SNR safety rod (A)

Position of axial traverse measured with SNEAK-platelets ( X )

Fission chambers (axially integrated fission rate is quoted) ( 100 )

Fig.9 Positions of the Axial Power Traverses measured in SNEAK-9A 2

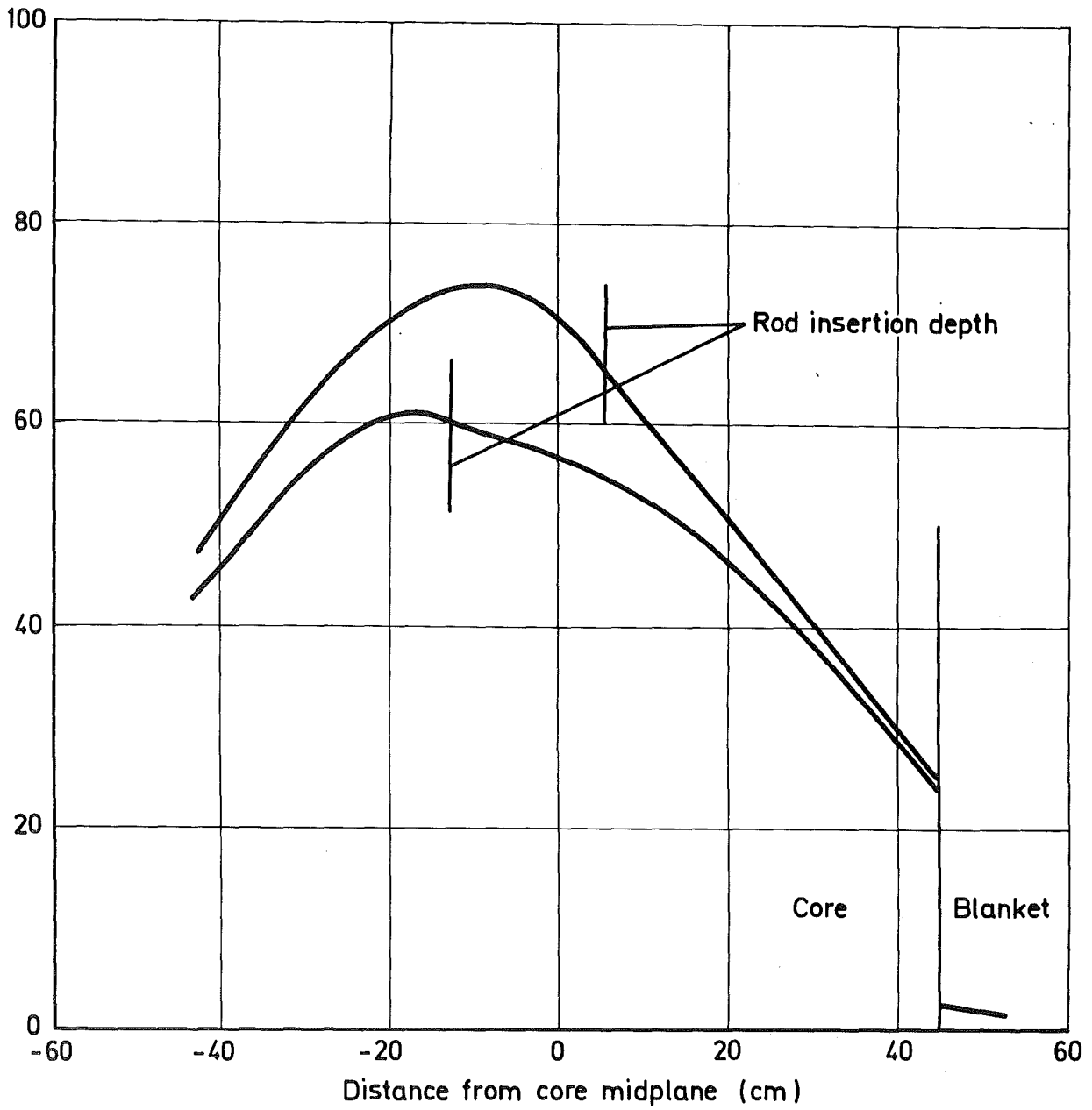
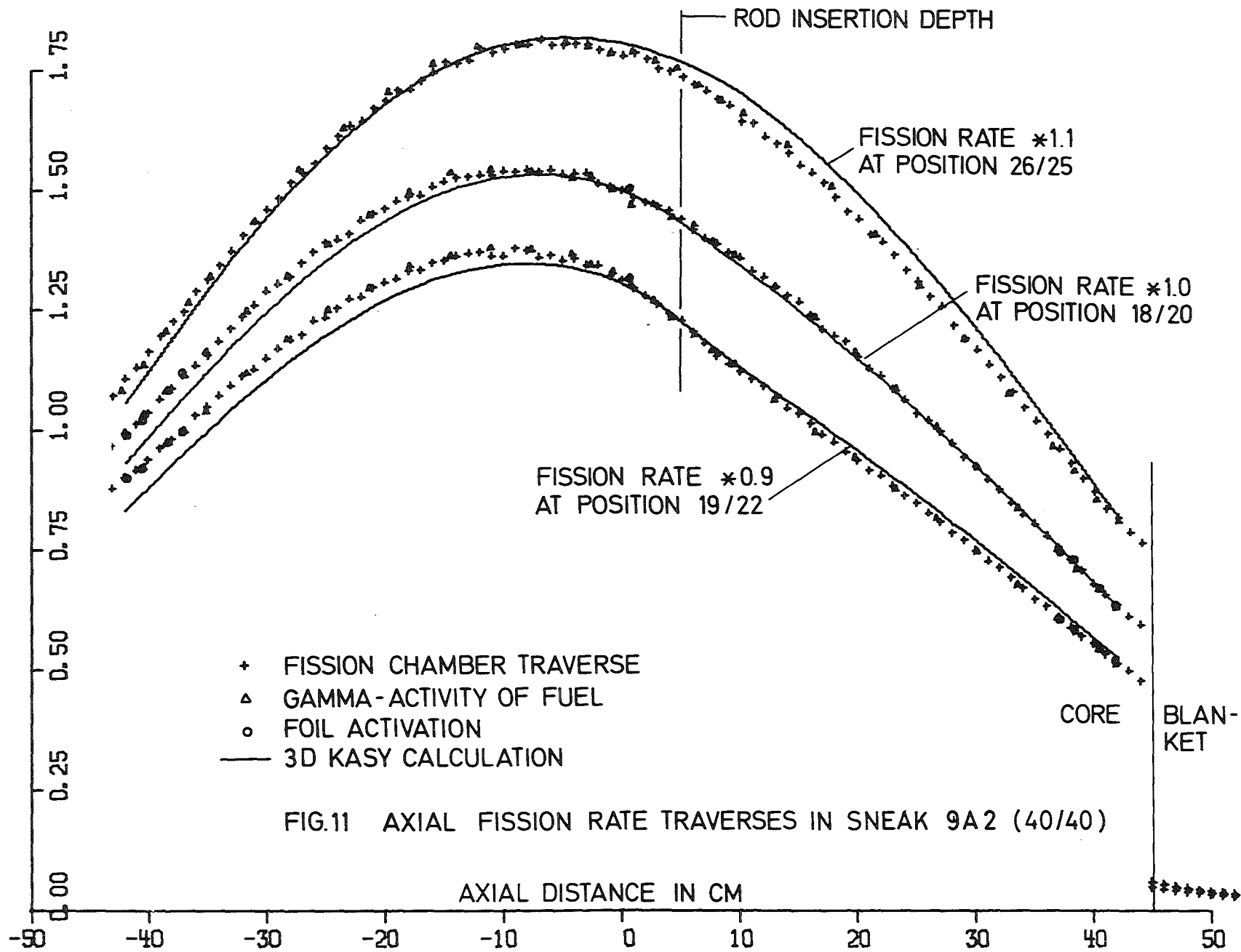


Fig. 10 Axial Power Traverses in SNEAK-9A2  
Position 19/22



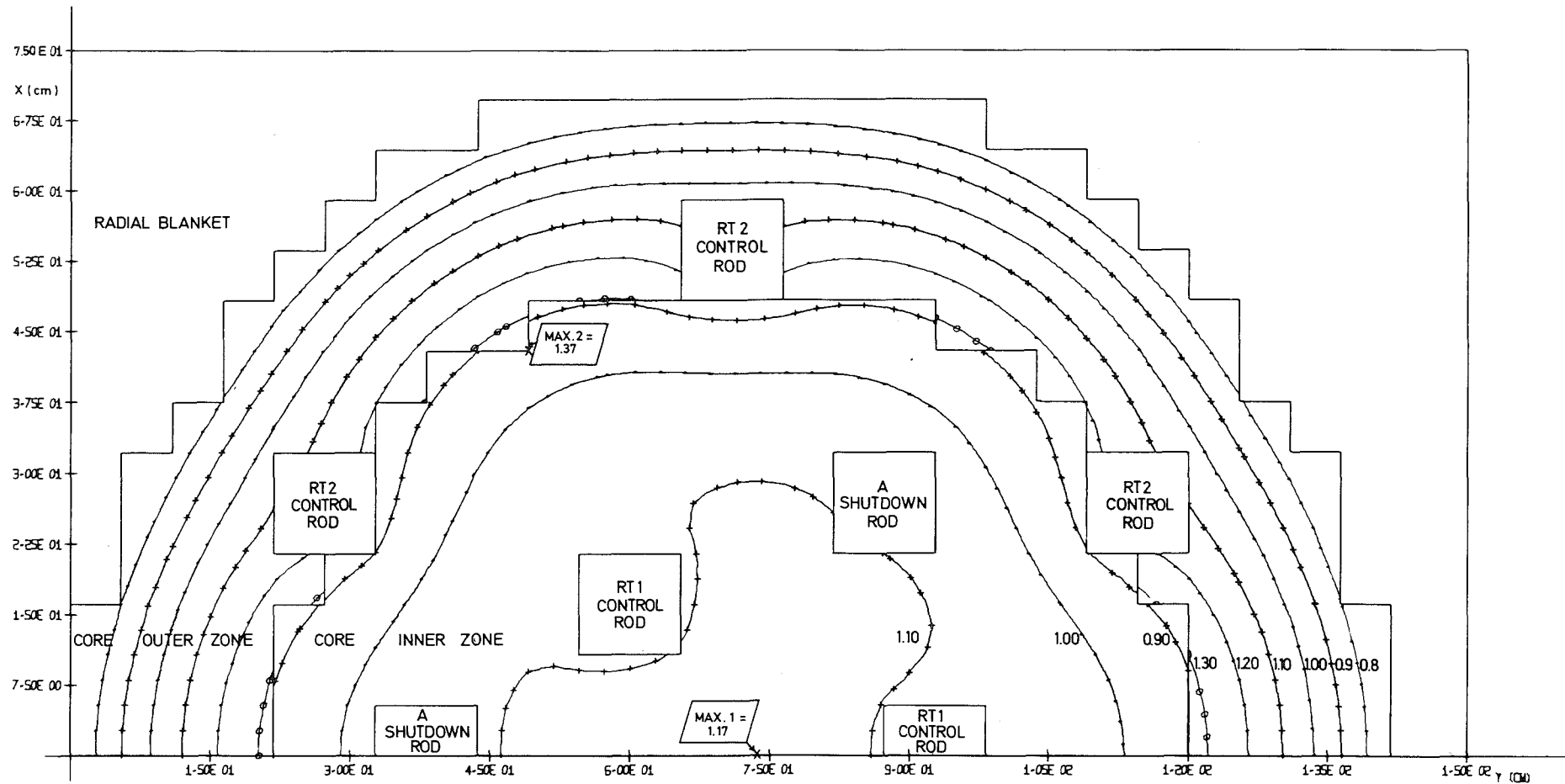


FIG. 12 SNEAK-9A2, FIRST CORE (40-40)  
TWO-DIMENSIONAL MAP OF AXIALLY INTEGRATED POWER VALUES (CALC)

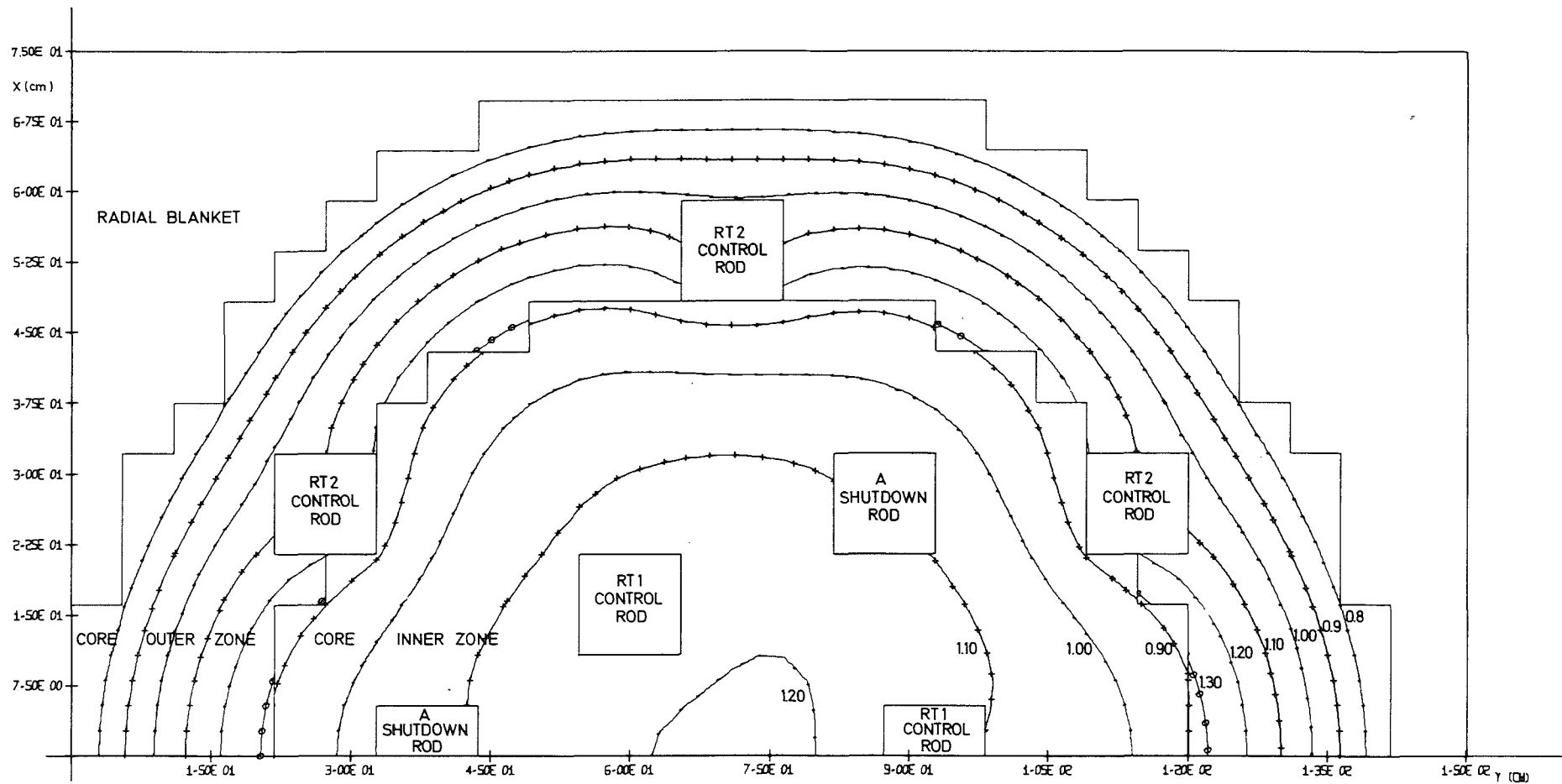


FIG. 13 SNEAK-9A2, SECOND CORE (28-50)  
TWO-DIMENSIONAL MAP OF AXIALLY INTEGRATED POWER VALUES (CALC)



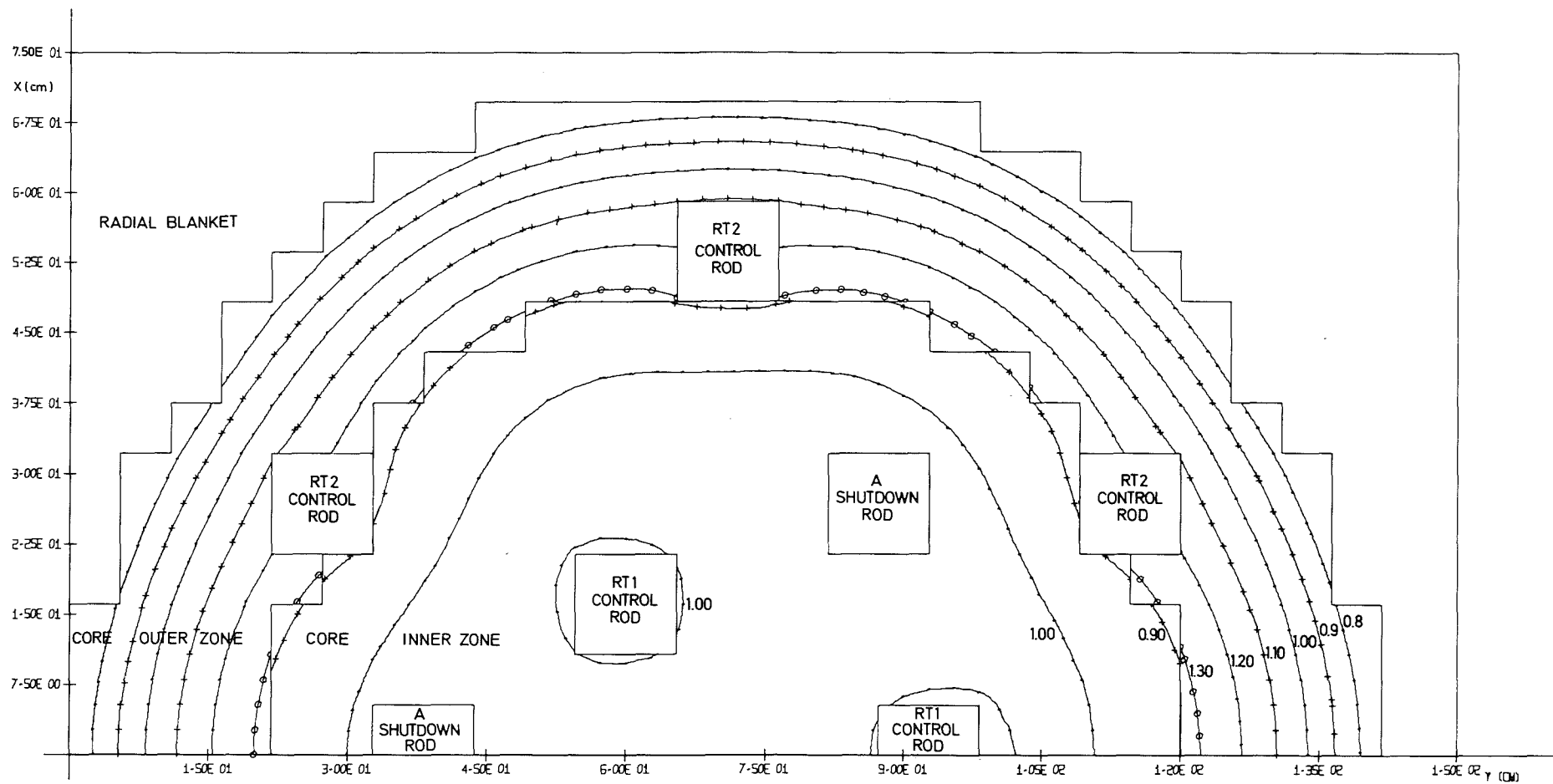
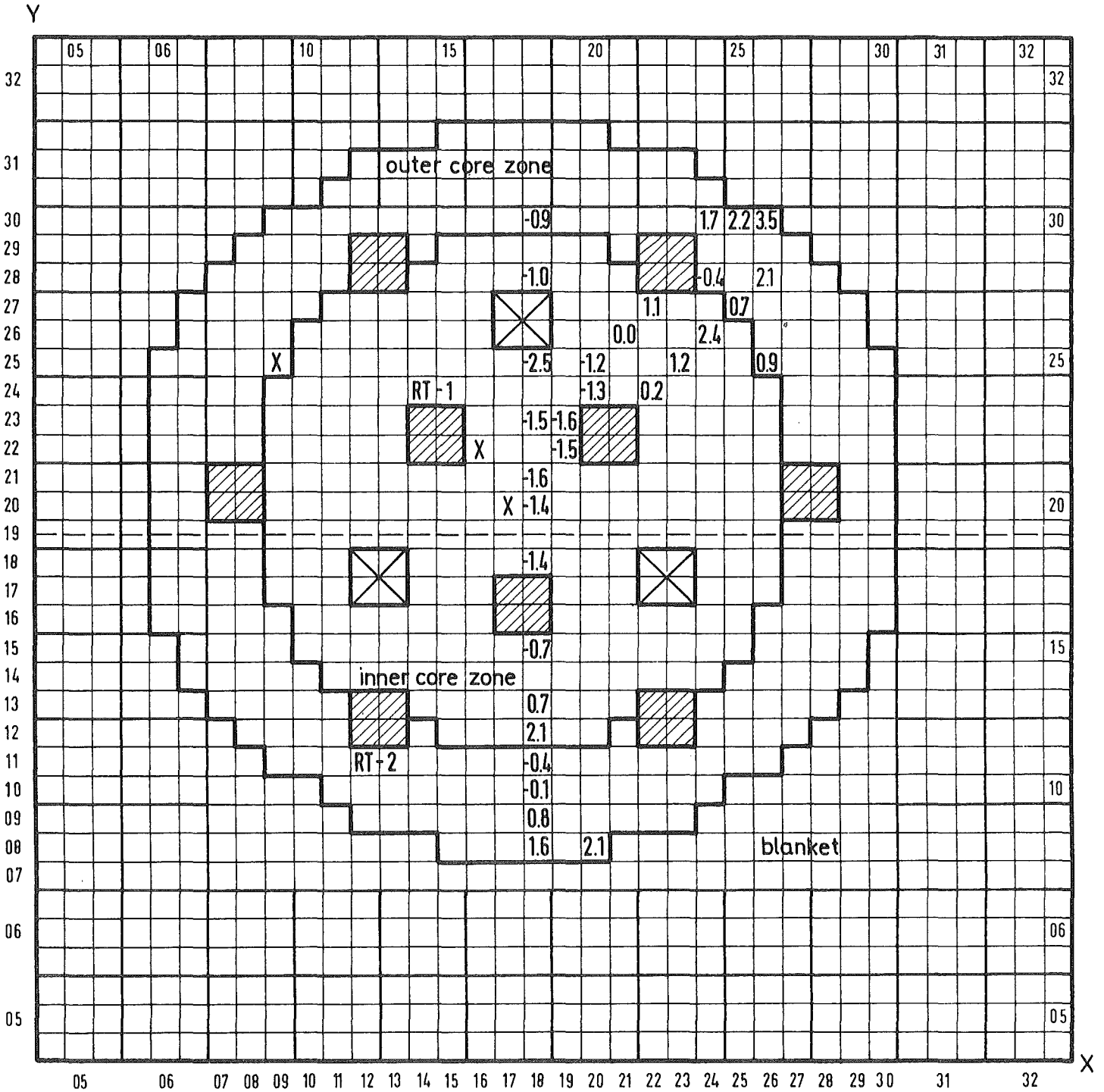


FIG. 14 SNEAK-9A2, THIRD CORE (58-20)  
TWO-DIMENSIONAL MAP OF AXIALLY INTEGRATED POWER VALUES (CALC)



SNEAK-9A2

First Core (40/40)

Relative Deviations of Axial Integrals

$$\left( \frac{C - E}{E} \text{ in } \% \right)$$

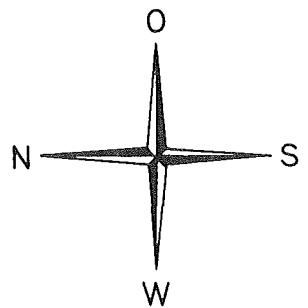
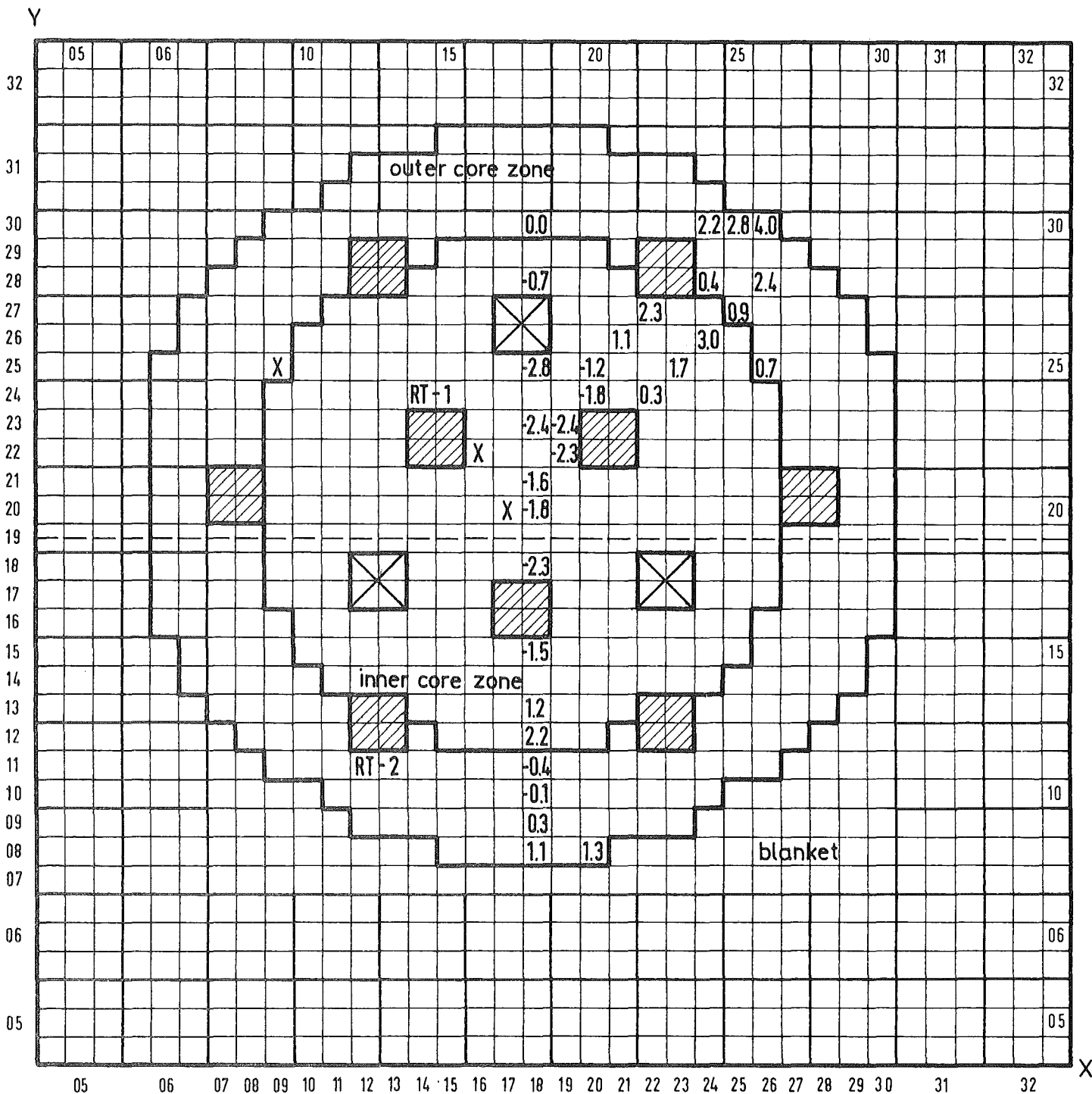


Fig. 15



SNEAK-9A2 Second Core (28/50)  
 Relative Deviations of Axial Integrals  
 $(\frac{C-E}{E} \text{ in } \%)$

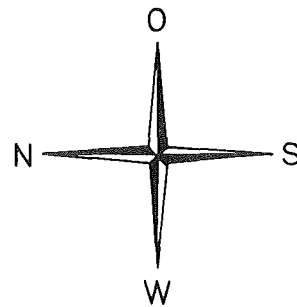
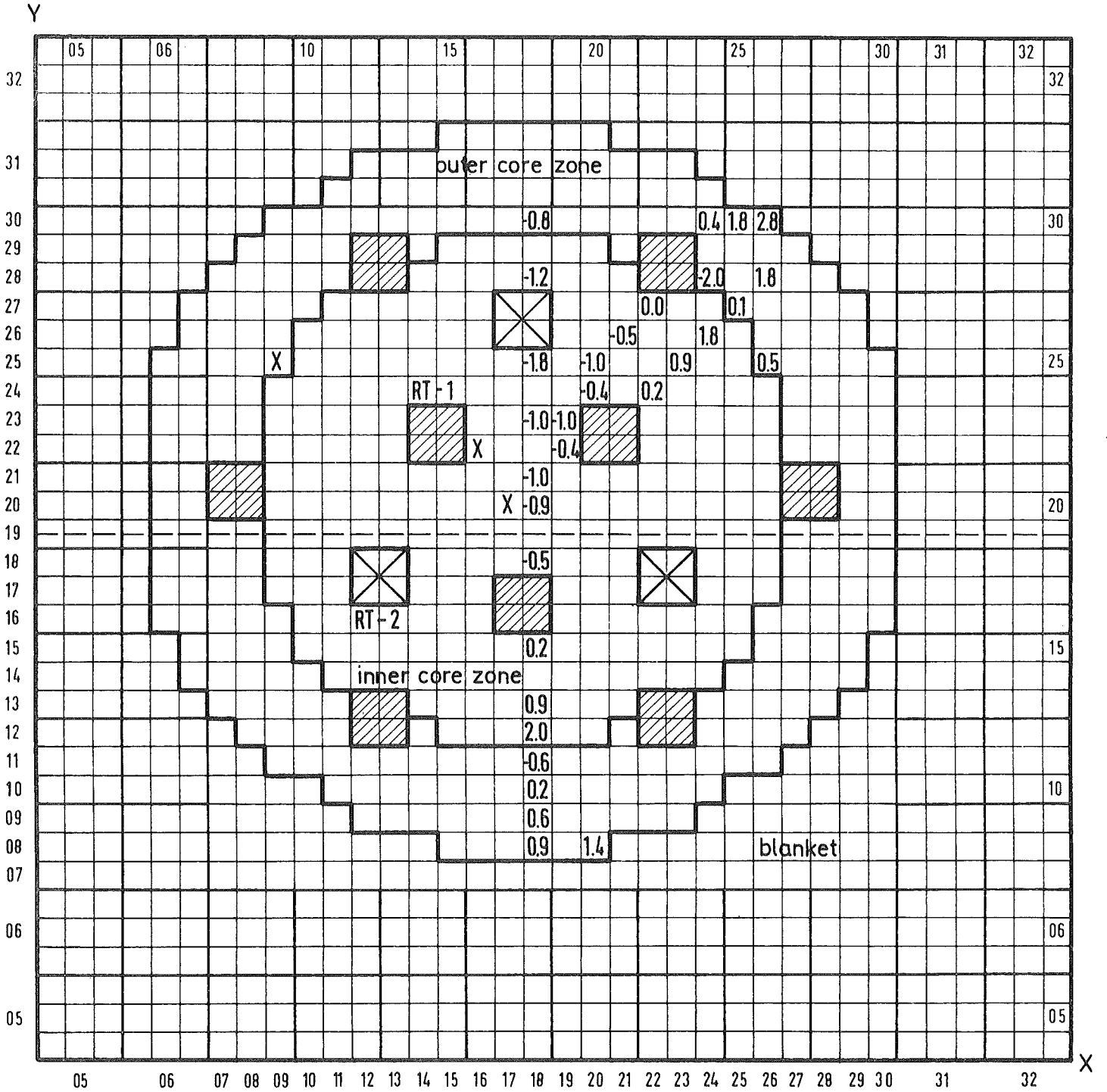


Fig. 16



SNEAK-9A2 Third Core (58 / 20)  
Relative Deviations of Axial Integrals  
( $\frac{C-E}{E}$  in %)

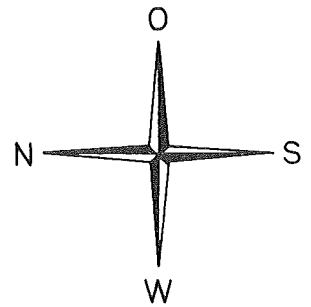


Fig. 17

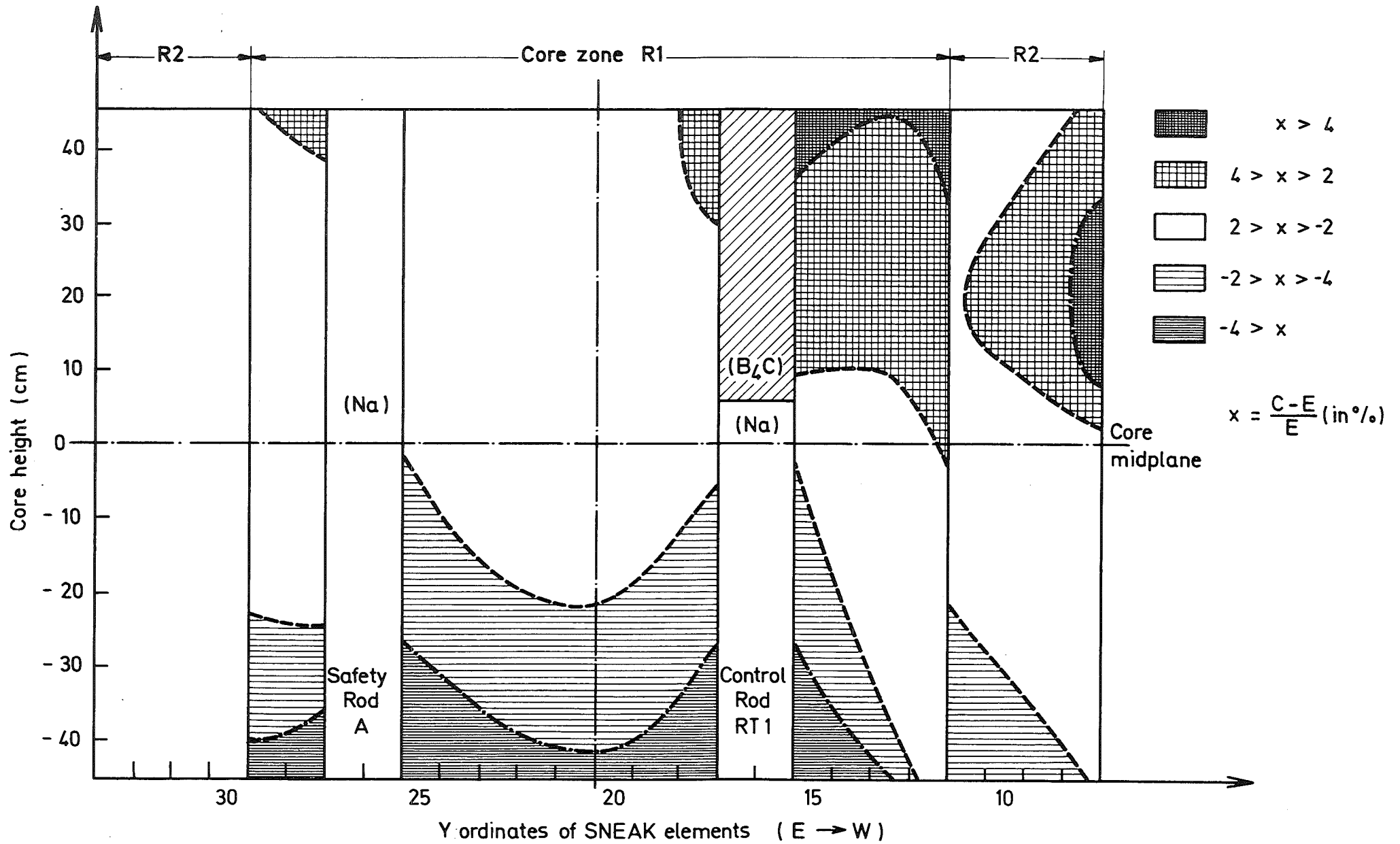


Fig. 18 Vertical cross section through SNEAK-9A 2 core (40/40) deviation of calculated power distribution from experiment

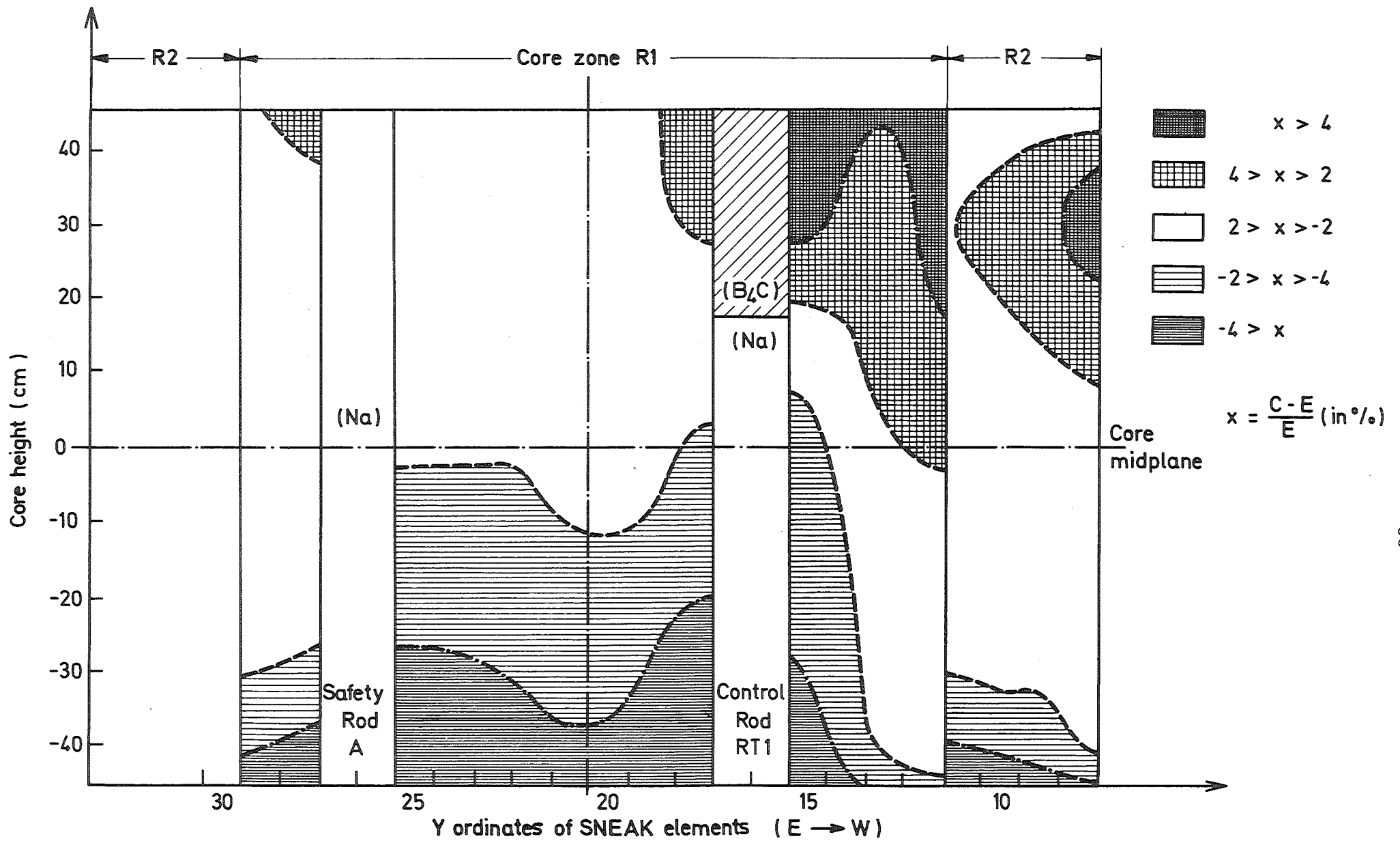


Fig.19 Vertical Cross Section through SNEAK - 9A 2 Core (28/50)  
 Deviation of Calculated Power Distribution from Experiment

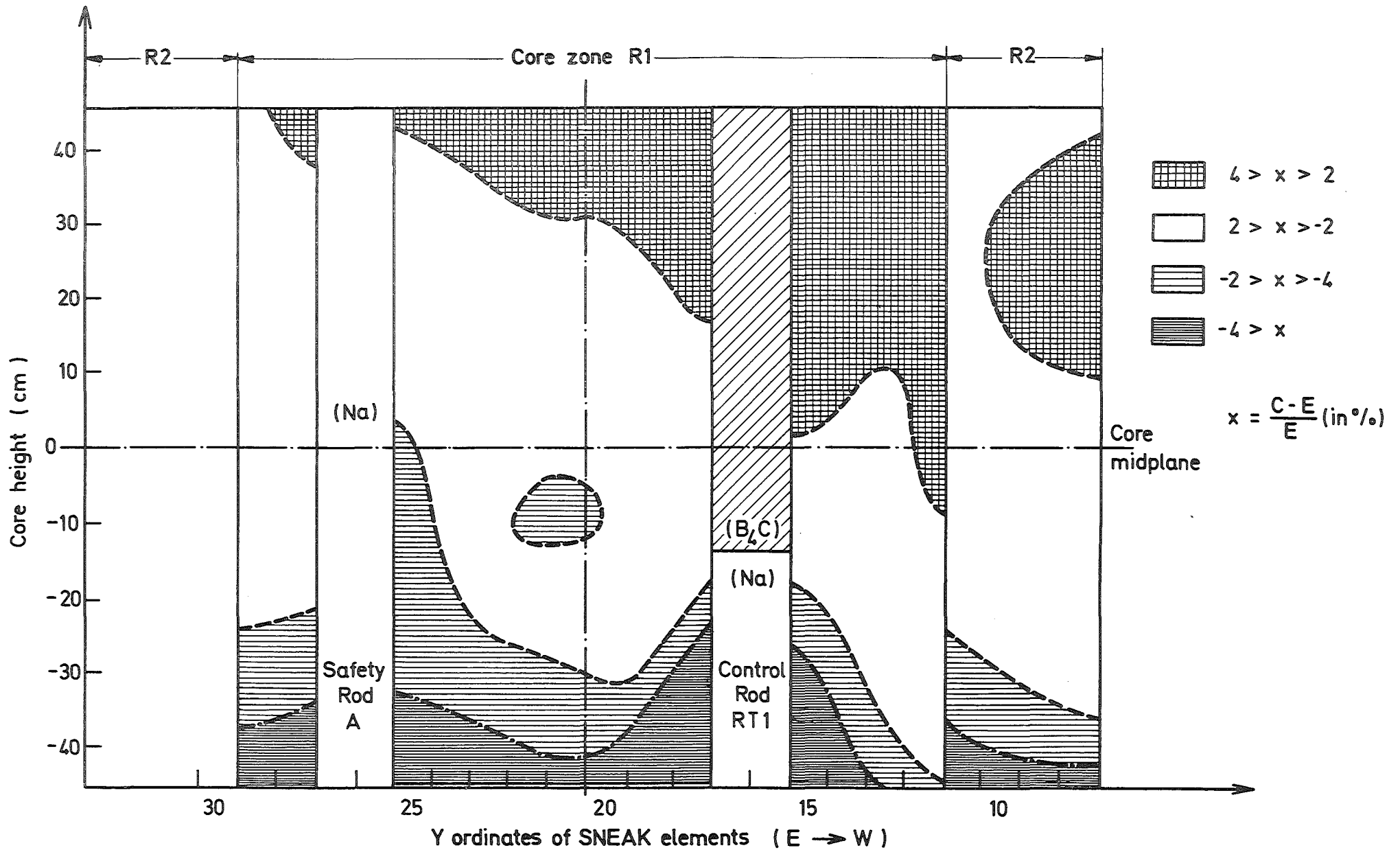


Fig. 20 Vertical Cross Section through SNEAK-9A2 Core (58/20)  
 Deviation of Calculated Power Distribution from Experiment